Ellipsometric study of critical adsorption and measurement of universal surface integrals

Dan S. P. Smith and Bruce M. Law
Department of Physics, Kansas State University, Manhattan, Kansas 66506-2601
(Received 11 March 1996; revised manuscript received 14 May 1996)

A recent study [D. S. P. Smith and B. M. Law, Phys. Rev. E **52**, 580 (1995)] presented the experimental determination of the universal critical adsorption integrals $\int P_+ = \int P_+(x)dx$ and $\int P_- = \int [P_-(x)-1]dx$, where $P_\pm(x)$ are the one-phase (+) and two-phase (−) universal functions that scale the variation of the local order parameter near a free surface in the vicinity of the Ising critical end point. In this previous ellipsometric study of the liquid-vapor surface of three binary liquid mixtures, the analysis assumed the surface layer to be composed purely of the preferentially adsorbed component and neglected capillary wave fluctuations. Here we present ellipsometric data for four liquid mixtures that were measured with improved temperature control. The analysis of the previous study is repeated on these data, and an effort is made to develop a method of analysis that is based on a more accurate set of assumptions. Measurements of the surface tension at the liquid-vapor surface of each mixture are used to estimate the surface layer's composition for each mixture. The ellipsometric data are analyzed assuming this calculated surface composition, and the contribution due to capillary waves is taken into account in an approximate fashion. The means of the $\int P_+$ and $\int P_-$ values obtained using the previous and current methods are not significantly different. This provides confidence that the experimentally determined values for $\int P_\pm$ are only slightly dependent on the above approximations, and that they have been determined with a high degree of accuracy. [S1063-651X(96)04609-0]

PACS number(s): 68.10.−m, 64.60.Fr, 05.70.Fh, 82.65.Dp

I. INTRODUCTION

Critical adsorption occurs at the liquid-vapor or liquid-solid surfaces in a critical binary liquid mixture when the bulk critical temperature T_c is approached from the one-phase side, and from the two-phase side provided a wetting layer does not form. For small reduced temperatures, $t=|T-T_c|/T_c \ll 1$, the thickness of the adsorption profile is scaled by the diverging bulk correlation length $\xi_\pm = \xi_{0\pm} t^{-\nu}$, where the subscript + (−) will be used to indicate one-phase (two-phase) quantities. Let L and H denote the two molecular components of the mixture, where L (H) represents the pure component with the lower (higher) density. The local order parameter is defined on the liquid side of the surface ($z \geqslant 0$) by

$$m(z,t) = \varphi_L(z,t) - \varphi_L(+\infty,0), \tag{1}$$

where $\varphi_L(z,t)$ is the local volume fraction of the L component expressed as a function of t and z, the depth into the liquid, while $\varphi_L(+\infty,0)$ is the bulk critical volume fraction. For the case in which L is preferentially adsorbed at the liquid-vapor surface (which requires that the surface tension of L is lower than the surface tension of H) the critical adsorption profile scales as [1–4]

$$m_\pm(z,t) = M_- t^\beta P_\pm\left(\frac{z+z_e}{\xi_\pm}\right). \tag{2}$$

The surface scaling functions $P_+(x)$ and $P_-(x)$ have different forms, but are both universal. Here β and M_- are the usual critical exponent and coefficient of the bulk order parameter in the two-phase region, where $m_-(+\infty,t) = M_- t^\beta$. The extrapolation length z_e is nonuniversal and independent of z. The surface scaling functions have the limits [2–4]

$$P_\pm(x) - P_\pm(\infty) \cong P_{\infty,\pm} e^{-x} \tag{3}$$

for $x \gg 1$, with $P_+(\infty)=0$ and $P_-(\infty)=1$, and

$$P_\pm(x) \cong c_\pm x^{-\beta/\nu} \tag{4}$$

for $x \ll 1$, where $P_{\infty,\pm}$ and $c_\pm$ are universal constants. A thorough and up to date review of the published experimental tests of the critical adsorption scaling equations (2), (3), and (4) is provided in Ref. [5].

Recent theories have provided values for $P_{\infty,\pm}$ and $c_\pm$, as well as numerical determinations of $P_\pm(x)$ in the crossover region between the limits of large and small x. Diehl and Smock [3] have published a renormalization-group, one-loop calculation for $P_\pm(x)$, while Smock, Diehl, and Landau [4] have fitted functions $P_\pm(x)$ to the Monte Carlo data of Landau and Binder [6]. In addition, Flöter and Dietrich [7] have provided universal quantities related to critical adsorption for dimension $d=3$ by interpolation of exact results for $d=2$ and $d=4$.

In a previous publication [8] we presented the experimental determination of the universal critical adsorption integrals

$$\int P_+ = \int_0^\infty P_+(x)dx, \tag{5a}$$

$$\int P_- = \int_0^\infty [P_-(x)-1]dx, \tag{5b}$$

and the ratio

$$R_{MA} = \int P_+ \Big/ \int P_- . \tag{5c}$$

From ellipsometric measurements on the liquid-vapor surface of the three critical binary liquid mixtures 2,6 lutidine-water (LW), nitrobenzene-hexane (NH), and 3 methylpyridine-D_2O (PD) we obtained $\int P_+ = 1.86 \pm 0.11$, $\int P_- = 1.61 \pm 0.04$, and $R_{MA} = 1.19 \pm 0.04$. The ellipsometric data on our samples of the critical mixtures LW and NH have since been remeasured using an improved thermostat, where thermal gradients have been minimized. Additional improved ellipsometric measurements on new samples of the critical liquid mixtures aniline-cyclohexane (AC) and isobutyric acid-water (IW) have been taken. The relevant experimental details are described in Sec. II, and the ellipsometric data for the mixtures AC, IW, LW, and NH are presented. In Sec. III the method of analysis developed in Ref. [8] is reviewed and applied to these data.

Ellipsometry measurements have contributions from both the static intrinsic profile expressed in Eqs. (1) and (2) and the thermally generated capillary wave fluctuations [9]. The analysis of the ellipsometric data in Ref. [8] and Sec. III of this manuscript considers only the intrinsic profile and neglects the capillary wave contribution. In addition, the analysis assumes the surface layer at $z = 0$ to be composed purely of the preferentially adsorbed component L, $\varphi_L(0,t) = 1$. This assumption is removed in Sec. IV, where we employ the semiempirical theory of Tamura, Kurata, and Odani [10] to derive an estimate for the surface volume fraction $\varphi_L(0,t)$ from liquid-vapor surface tension measurements. In Sec. V we discuss an approximation by which the capillary wave contribution to the ellipsometry measurements can be taken into account. The analysis developed in Secs. IV and V is applied to the ellipsometric data for the mixtures AC, IW, LW, and NH in Sec. VI, and conclusions are drawn from the results of this and other methods of analysis. Finally, Sec. VII summarizes the paper.

II. EXPERIMENTAL DETAILS

Phase-modulated ellipsometry [11] is a particularly effective method for probing the order-parameter profile. A procedure established by Beaglehole [12] is to monitor the coefficient of ellipticity at the Brewster angle, defined by

$$\overline{\rho} = \mathrm{Im}(r_p / r_s)|_{\theta_B}, \tag{6}$$

where r_p and r_s are the complex reflection coefficients for the two independent polarizations. Our ellipsometric study of the critical mixtures AC, IW, LW, and NH was originally reported in Refs. [13] and [14] and $(\overline{\rho},t)$ data for the mixtures LW and NH were presented in Ref. [8]. For the reasons discussed in this section below, new samples have been prepared for the mixtures AC and IW, and $(\overline{\rho},t)$ data have been measured for all four mixtures with improved accuracy for the present publication.

The four liquid mixtures were chosen in part because they do not form a wetting layer in the two-phase region. This requires that the component L have the lower liquid-vapor surface tension. Each of the four mixtures has been the focus of several past experimental studies of bulk critical phenomena. In Table I selected literature values for the critical volume fraction of component L, $\varphi_L(+\infty,0)$, and the critical temperature T_c are given for each of the four mixtures. These values are provided so that they may be compared with our measured values, and will not be used in the analysis below.

TABLE I. Literature values for the critical volume fraction and the critical temperature. These values are provided so that they may be compared with our measured values in Table II.

Mixture	$\varphi_L(+\infty,0)$	T_c (Kelvin)
AC[a]	0.598	303.45
IW[b]	0.401	299.14
LW[c]	0.3073	306.75
NH[d]	0.623	293

[a]Reference [48].
[b]Reference [49].
[c]Reference [50].
[d]Reference [51].

Trace levels of water or other impurities can shift the critical temperature of binary liquid mixtures by as much as several degrees, and can affect certain other bulk properties significantly. Chemical purity could be even more important for surface measurements because of the possibility of preferential adsorption of the impurities. The purification procedures used for each of the chemicals were discussed in Ref. [14]. The cells containing the samples were composed entirely of Pyrex. They were cleaned with an acid glass etch, rinsed in deionized, distilled water, and oven dried overnight in air. After being filled, the cells were flame sealed. As a test of the purity of our samples, the literature T_c values listed in Table I can be compared with the values measured for our samples, given in Table II. Each of the literature values for T_c agrees with our measured values to within 0.5 °C.

The most reliable method of checking that a sample has been mixed at the critical concentration is to verify that after a quench from a one-phase temperature to a two-phase temperature near T_c, the meniscus forms in the middle of the sample cell, dividing the two phases into equal volumes. This test of criticality was performed for both the samples of LW and NH in Ref. [14], but not for the samples of AC and IW reported in Ref. [13]. New samples of the mixtures AC and IW were prepared and checked for criticality for this paper. The values of $\varphi_L(+\infty,0)$ given in Table II differ from the old values reported in Ref. [8] by 8% and 3% for AC and IW, respectively.

A conventional phase-modulated ellipsometer, based on the design of Beaglehole [12] and incorporating a high stability birefringence modulator [15], was used for the $\overline{\rho}$ measurements. A He-Ne laser ($\lambda = 633$ nm) was employed as the light source. The formation of the liquid-liquid meniscus could not be observed while the sample cells were in the ellipsometer's thermostat. Instead the critical temperature T_c was measured by visual observation of the scattering of a He-Ne laser beam passing through the sample. As the temperature is slowly varied from the one-phase region into the two-phase region, the onset of phase separation is marked by heavy scattering of the beam.

The sample cells were half-filled Pyrex cylinders with ap-

TABLE II. Nonuniversal bulk parameters required for the analysis of the four critical liquid mixtures studied in this paper.

Mixture	ϵ_L [a]	ϵ_H [a]	M_-	ξ_{0+} (Å)	$\varphi_L(+\infty,0)$ [b]	T_c (Kelvin) [b]
AC	2.035	2.5163	1.03 ± 0.03 [c]	2.3 ± 0.2 [d]	0.592 ± 0.001	303.049 ± 0.003
IW	1.94	1.773	0.783 ± 0.03 [e]	3.63 ± 0.07 [f]	0.405 ± 0.01 [g]	299.099 ± 0.003
LW	2.217 [h]	1.773	0.931 ± 0.007 [i]	2.5 ± 0.3 [j]	0.308 ± 0.001	306.579 ± 0.004
NH	1.8909	2.4218	0.770 ± 0.006 [k]	3.1 ± 0.4 [l]	0.623 ± 0.002	293.107 ± 0.004

[a]Reference [52], except were noted.
[b]Measured for this publication.
[c]References [53,54].
[d]References [53,48].
[e]Reference [20].
[f]Reference [53].
[g]Reference [8].
[h]Reference [55].
[i]Reference [56].
[j]Reference [57].
[k]References [54,51].
[l]Reference [58].

proximate lengths and inner diameters of 6.5 and 2.3 cm, respectively. Inside the thermostat a cell was laid with its axis horizontal and precision thermistors [16] monitored its temperature at both ends, which will be denoted by T_1 and T_2. Using electronics that are able to resolve a fraction of a mK changes in a thermistor's temperature, the resistance-temperature curves of the two thermistors were determined to be matched to within a few mK. This allowed the fluctuations in T_1 and T_2 to be measured with an accuracy of better than 1 mK, and the gradient along the cell's axis to be determined with an accuracy of better than 1 mK/cm. It was discovered that the thermostat used to produce the $(\overline{\rho},t)$ data in Refs. [8], [13], and [14] causes a gradient of several mK/cm along the sample cell axis. The data for the present paper were measured with the sample cell's temperature controlled by a new thermostat, which, with care, can maintain gradients of less than 1 mK/cm. Both the old and new thermostats hold the temperatures T_1 and T_2 stable to within 1 mK. The laser beam probed the liquid halfway between the two ends of the cell. Thus the mean value $T=(T_1+T_2)/2$ was used for the temperature of the sample, and $\Delta T=(T_1-T_2)/2$ was used as a conservative estimate of the uncertainty on the temperature measurement due to the presence of the gradient.

The procedure used for the ellipsometry measurements consisted of setting the temperature, waiting for thermal and diffusive equilibrium, then taking 20 measurements of $(\overline{\rho},T,\Delta T)$ over the succeeding 2 h. From this set of 20 measurements the mean of $\overline{\rho}$ and its standard deviation were determined. The mean of T was used for the temperature, and for its uncertainty the larger of one standard deviation of T and the mean of ΔT was used. The mean of ΔT, which is an estimate of the uncertainty due to the temperature gradient across the sample cell, was nearly always larger than the standard deviation of T, which is the uncertainty due to temperature fluctuations. The typical wait time for diffusive equilibrium was 2 h beyond the establishment of thermal equilibrium; this was increased to as much as 8 h near T_c, where diffusion is slowed asymptotically. As a check on the sufficiency of these wait times, the variation of $\overline{\rho}$ was occasionally monitored over 24 h periods. The temperature was always stepped from the one-phase region to the two-phase region, so that gravity assisted the phase separation process. When it was necessary to return to a homogeneous single phase above T_c (below T_c for the lower critical mixture LW), the sample was heated well into the one-phase region and thoroughly shaken after thermal equilibrium had been established. To avoid problems associated with a slow T_c drift, temperatures within 20 mK of T_c were measured in the span of a few days immediately following the measurement of T_c. The average T_c drift for the mixture NH was determined to be approximately 0.5 mK/day, but was not measured for the other three samples. The initial scan was followed by scans of successively larger temperature intervals about T_c. Different scans showed a reproducibility in $\overline{\rho}$ that was typically better than 5×10^{-5}.

The $(\overline{\rho},t)$ data for the mixtures AC, IW, LW, and NH are presented in Tables IV, V, VI, and VII, respectively. For the mixtures LW and NH the $(\overline{\rho},t)$ data fell on top of the previous data reported in Ref. [8] for $t\gtrsim10^{-3}$, and the previous data in this range has been included with the current data in Tables VI and VII of this manuscript. For $t\lesssim10^{-3}$ the previous data deviates significantly from the current data, indicating that the larger temperature gradient was an important source of error to the measurements at small reduced temperatures. The uncertainty on the measured value of T was estimated for each of the current data points as discussed above. From this the value for the uncertainty on the measured value of the reduced temperature t was determined, and is provided for each of the current data points given in Tables IV, V, VI, and VII. The gradient across the sample cell was not measured for each of the previous data points reported in Ref. [8], but it was recently measured in our previous thermostat under normal operating conditions. Because of this, a single estimated value of 5×10^{-5} is given in Tables VI and VII for the uncertainty of t for all of the previous data points. This uncertainty is small compared to the large reduced temperatures of the previous data that have been retained. For the mixtures AC and IW the current results are for samples of slightly different concentrations than the samples studied in Ref. [13], and the previous and current $(\overline{\rho},t)$ curves do not agree until $t\gtrsim10^{-2}$. The data reported for the mixtures AC and IW in Tables IV and V do not contain any of the previous data.

III. THE STATIC INTRINSIC PROFILE

For thin surface profiles (compared to the wavelength of light, $\lambda=633$ nm) the contribution of the static intrinsic sur-

face profile (ip) to the ellipsometric coefficient $\overline{\rho}$ is described by the Drude equation [17],

$$\overline{\rho_{\rm ip}} = -\frac{\pi}{\lambda}\frac{\sqrt{\epsilon(+\infty,t)+\epsilon(-\infty,t)}}{\epsilon(+\infty,t)-\epsilon(-\infty,t)} \times \int_{-\infty}^{+\infty}\frac{[\epsilon(z,t)-\epsilon(+\infty,t)][\epsilon(z,t)-\epsilon(-\infty,t)]}{\epsilon(z,t)}dz, \tag{7}$$

where $\epsilon(z,t)$ is the optical dielectric profile of the reflecting medium. The Drude equation (7) is only valid for surface profile thicknesses that are thin compared to λ. Since z is scaled by ξ in Eq. (2), this corresponds to $\xi \ll \lambda$, which occurs far from T_c. For thicker profiles (smaller reduced temperatures), Maxwell's equations have to be solved numerically [5,18,19]. In this paper and in Ref. [8] the Drude equation is used to analyze the $(\overline{\rho},t)$ data far from T_c. A numerical analysis over the entire range of t is the subject of Ref. [5].

The use of Eq. (7) in the analysis of the $(\overline{\rho},t)$ data requires the development of a model optical dielectric profile $\epsilon(z,t)$. The static intrinsic profile at the liquid-vapor surface of a liquid mixture consists of both a composition profile and the variation of the total number density of molecules from its effectively zero value in the bulk vapor to the much denser bulk liquid value. We have studied liquid mixtures near 1 atm pressure and under 60 °C, which is far from the *liquid-vapor* critical point where the total number density profile undergoes critical scaling and becomes very thick. For this reason the total number density profile will be referred to as the noncritical profile, and previous analysis and experiments [8,19] on critical liquid mixtures have found it to be only a few molecular layers thick. For critical binary liquid mixtures near the liquid-liquid critical temperature the thickness of the composition profile, to be referred to as the critical profile, diverges proportionally to the correlation length ξ. In the reduced temperature ranges analyzed in this paper, ξ is 10 to 100 molecular layers thick, so that the noncritical profile is from 10% down to a fraction of a percent of the thickness of the critical profile. This suggests that the nonzero thickness of the noncritical profile should not cause the critical profile to deviate significantly from Eq. (2).

The critical profile is expressed quantitatively in terms of the local order parameter $m(z,t)$ defined in Eq. (1). It is commonly converted to the optical dielectric profile $\epsilon(z,t)$ by the use of the two-component Clausius-Mossotti relation, [20],

$$\varphi_L(z,t)\,\eta_L + [1-\varphi_L(z,t)]\,\eta_H \cong \eta(z,t), \tag{8}$$

where volume changes on mixing, which are typically only 1–2% for most mixtures, have been ignored. In Eq. (8) for $i=L$ and H,

$$\eta_i = \frac{\epsilon_i - 1}{\epsilon_i + 2}, \tag{9}$$

where ϵ_i is the optical dielectric constant of pure liquid i, and

$$\eta(z,t) = \frac{\epsilon(z,t)-1}{\epsilon(z,t)+2}. \tag{10}$$

In Ref. [8] the Clausius-Mossotti relation (8) was used to convert the critical profile expressed in terms of volume fraction in Eqs. (1) and (2) into an optical dielectric profile,

$$\epsilon(z,t) = \frac{1+2[\Delta(z,t)+\eta(+\infty,t)]}{1-[\Delta(z,t)+\eta(+\infty,t)]}, \quad z \geqslant 0, \tag{11}$$

where

$$\Delta(z,t) = (\eta_L - \eta_H) M_- t^{\beta}\left[P_{\pm}\left(\frac{z+z_e}{\xi_{\pm}}\right) - P_{\pm}(\infty)\right]. \tag{12}$$

Near the surface ($x \ll 0$) on the liquid side, the surface scaling functions $P_{\pm}(x)$ can be approximated by the power law of Eq. (4). Therefore from Eqs. (1) and (2) we obtain the result

$$\varphi_L(z,t) = \varphi_L(+\infty,0) + M_- c_{\pm}\left(\frac{z+z_e}{\xi_{0\pm}}\right)^{-\beta/\nu}, \quad \frac{z+z_e}{\xi_{\pm}} \ll 1. \tag{13}$$

This demonstrates that the only t dependence of the composition of the liquid near the surface is due to the possible t dependence of z_e. Because of this it seems reasonable to formulate a noncritical profile that has an explicit z_e dependence, but to otherwise neglect any variation in the noncritical profile with t that might be induced by the varying composition on the liquid side of the surface. The ranges of temperature and pressure in our experiment are very small compared to the separation from the temperature and pressure at the *liquid-vapor* critical point. We therefore assume that the noncritical profile does not vary with temperature, except for the possible variation of z_e with t.

Numerical calculations [5,19] have shown that if the noncritical profile is independent of the temperature, its contribution to $\overline{\rho}$ is nearly independent of t regardless of the functional form assumed for the z dependence of the noncritical profile. This allows the use of a simple one-adjustable-parameter model for the noncritical profile, because with a suitable choice of the adjustable parameter the simple model will contribute nearly the same approximately constant reduced temperature dependence to $\overline{\rho}$ as will a more elaborate model. To simplify the analysis in Ref. [8] the noncritical profile was confined to the vapor side of the surface ($z \leqslant 0$). The Fermi interfacial profile expected in mean-field theory [21] was modified to give the optical dielectric profile

$$\epsilon(z,t) = 1 + \frac{[\epsilon(0,t)-1][1+e^{-z_e/\xi_v}]}{1+e^{-(z+z_e)/\xi_v}}, \quad z \leqslant 0, \tag{14}$$

where the vapor correlation length ξ_v scales the noncritical profile thickness.

Equations (11) and (14) describe the model optical dielectric profile that will be used, but they contain many nonuniversal parameters that must be specified for each mixture. For this reason we have chosen to study only mixtures that are well documented experimentally in the literature. The values used for ϵ_L, ϵ_H, M_-, ξ_{0+}, and $\varphi_L(+\infty,0)$ are pro-

TABLE III. Parameters measured for the bulk index of refraction of the four critical liquid mixtures as a function of the reduced temperature. The index of refraction has the functional form $n(t)=n_c+n_1t+n_\alpha t^{1-\alpha}$ in the one-phase region, and $n(t)=n_c-n_1t+2n_\alpha t^{1-\alpha}+n_\beta t^\beta(1+n_\Delta t^\Delta)$ in the two-phase region.

Mixture	n_c	n_1	n_α	n_β	n_Δ
AC[a]	1.502	−0.157	−0.007	−0.157	0
IW[b]	1.356	−0.0738	0	0.048	0
LW[c]	1.3772	0.08	0	0.144	0
NH[d]	1.444	−0.164	0.0116	−0.14	0.4

[a]Reference [53].
[b]Reference [20].
[c]References [56,50].
[d]Reference [51].

vided in Table II. We are relying on literature values for all of these parameters except $\varphi_L(+\infty,0)$. The correlation length in the two-phase region, ξ_{0-}, was determined with the relation [22]

$$\xi_{0+}/\xi_{0-}=1.96. \tag{15}$$

The relation $\epsilon=n^{1/2}$ was used to determine $\epsilon(+\infty,t)$, where n is the refractive index of the bulk liquid mixture provided in Table III and is also taken from the literature. The surface optical dielectric constant $\epsilon(0,t)$ can be expressed in terms of the surface volume fraction $\varphi_L(0,t)$ using Eqs. (8), (9), and (10) with $z=0$. Using this value of $\epsilon(0,t)$ in Eq. (14) imposes continuity (but not smoothness) of $\epsilon(z,t)$ at $z=0$. The extrapolation length z_e appearing in both Eqs. (12) and (14) can also be expressed in terms of the surface volume fraction $\varphi_L(0,t)$. If $z_e \ll \xi_\pm$, Eq. (13) provides the analytic result

$$z_e=\xi_{0\pm}\left(\frac{\varphi_L(0,t)-\varphi_L(+\infty,0)}{M_-c_\pm}\right)^{-\nu/\beta}. \tag{16}$$

Outside the applicability of this limit, z_e must be determined from $\varphi_L(0,t)$ numerically using Eqs. (1) and (2) at $z=0$. This leaves $\varphi_L(0,t)$ and ξ_v as the only two unknown quantities in Eqs. (11) and (14).

In Ref. [8] the optical dielectric profile expressed in Eqs. (11) and (14) was used in the Drude equation (7) to derive the nearly exact result

$$\overline{\rho_{\rm ip}}=\overline{\rho_{\rm bg,ip}}-\frac{\pi}{\lambda}f_\epsilon(t)(\eta_L-\eta_H)M_-\xi_{0\pm}(\textstyle\int P_\pm)t^{\beta-\nu}. \tag{17}$$

The intrinsic profile background term $\overline{\rho_{\rm bg,ip}}$ has a weak, nondiverging dependence on t, and is given by

$$\overline{\rho_{\rm bg,ip}}=\overline{\rho_{\rm nc}}-\frac{\pi}{\lambda}f_\epsilon(t)(\eta_L-\eta_H)M_-\xi_{0\pm}[I_1(t)+I_2(t)], \tag{18}$$

where the functions $f_\epsilon(t)$, $I_1(t)$, and $I_2(t)$ are given in Eqs. (A4), (A8), and (A9) of Ref. [8]. The contribution of the noncritical profile of Eq. (14) to $\overline{\rho_{\rm ip}}$ is contained in the term $\overline{\rho_{\rm nc}}$. Equations (B3), (B6), and (B7) of Ref. [8] can be used to provide the explicit expression

$$\overline{\rho_{\rm nc}}=-\frac{\pi}{\lambda}\sqrt{\epsilon(+\infty,t)+1}\,\frac{\epsilon(0,t)-1}{\epsilon(+\infty,t)-1}(1+e^{-z_e/\xi_v})\xi_v\left\{\ln(1+e^{z_e/\xi_v})-\frac{\epsilon(+\infty,t)}{\epsilon(0,t)+[\epsilon(0,t)-1]e^{-z_e/\xi_v}}\ln[\epsilon(0,t)(1+e^{z_e/\xi_v})]\right\}. \tag{19}$$

The surface volume fraction $\varphi_L(0,t)$ must be determined in order that z_e and $\epsilon(0,t)$ can be determined. In Ref. [8] it was assumed that the surface layer is pure L, $\varphi_L(0,t)=1$. This assumption is the subject of Sec. IV. It was proposed in Ref. [8] that if this assumption is true, then the noncritical profile for $z\leq 0$ should be approximately the same as the liquid-vapor profile of pure L. This allowed the vapor correlation length ξ_v to be determined from the ellipsometric measurement on the liquid-vapor surface of pure L, $\overline{\rho_{\rm pure}}$. The relation between the two is given by Eq. (B3) of Ref. [8]. Equation (19) can then be rewritten as

$$\overline{\rho_{\rm nc}}=\sqrt{\frac{\epsilon(+\infty,t)+1}{\epsilon(0,t)+1}}\,\frac{\epsilon(0,t)-1}{\epsilon(+\infty,t)-1}[1+R_v(t)]\overline{\rho_{\rm pure}}, \tag{20}$$

where

$$R_v(t)=\frac{[\epsilon(0,t)-\epsilon(+\infty,t)]\ln[\epsilon(0,t)(1+e^{z_e/\xi_v})]}{[\epsilon(0,t)-1]e^{-z_e/\xi_v}\ln(1+e^{z_e/\xi_v})-\epsilon(0,t)\ln[\epsilon(0,t)]}. \tag{21}$$

Equation (17) is based upon the Drude equation (7), which is only valid in the limit of thin profiles compared with the wavelength of light λ. In Ref. [8] the range of t over which Eq. (17) is valid for each mixture was determined by comparing the $(\overline{\rho},t)$ curves calculated from Eqs. (17), (18), (20), and (21) with effectively exact numerical results. Nonlinear least-squares regression [23] was then used to fit the $(\overline{\rho},t)$ experimental data for the mixtures LW, NH, and PD to Eqs. (17), (18), (20), and (21) over these ranges of t. First the universal integrals $\int P_\pm$, $\overline{\rho_{\rm pure}}$, and the critical exponent $\beta-\nu$ were fitted. Because the factor $t^{\beta-\nu}$ stands out as the only quantity that diverges as $t\to 0$ in Eq. (17), it was determined that $\int P_\pm$ and $\beta-\nu$ could be fitted with reasonable precision. Next $\int P_\pm$ and $\overline{\rho_{\rm pure}}$ were fitted with $\beta-\nu$ held fixed at its theoretical value of -0.304 ($\beta=0.328$ and $\nu=0.632$), in order to determine $\int P_\pm$ with greater precision. The fitted values of $\overline{\rho_{\rm pure}}$ were in reasonable agreement with the actual measured values, which gave additional support for the model. In the current manuscript we will call this fit model I.

Model I has been applied to the improved $(\overline{\rho},t)$ data sets for the mixtures AC, IW, LW, and NH, which are provided

TABLE IV. Ellipsometric data as a function of the reduced temperature for the critical liquid mixture aniline-cyclohexane (AC).

t (one-phase region)	$10^3\overline{\rho}$	t (two-phase region)	$10^3\overline{\rho}$
$4.019\times10^{-2}\pm5\times10^{-5}$	2.518 ± 0.140	$9.128\times10^{-3}\pm3\times10^{-5}$	1.781 ± 0.132
$4.018\times10^{-2}\pm5\times10^{-5}$	2.566 ± 0.220	$8.131\times10^{-3}\pm3\times10^{-5}$	1.846 ± 0.103
$3.354\times10^{-2}\pm4\times10^{-5}$	2.634 ± 0.195	$7.470\times10^{-3}\pm3\times10^{-5}$	1.878 ± 0.066
$3.353\times10^{-2}\pm4\times10^{-5}$	2.810 ± 0.270	$6.813\times10^{-3}\pm3\times10^{-5}$	1.901 ± 0.238
$2.688\times10^{-2}\pm4\times10^{-5}$	2.861 ± 0.165	$6.344\times10^{-3}\pm1\times10^{-5}$	1.974 ± 0.114
$2.355\times10^{-2}\pm4\times10^{-5}$	2.905 ± 0.129	$6.342\times10^{-3}\pm1\times10^{-5}$	1.990 ± 0.017
$2.022\times10^{-2}\pm3\times10^{-5}$	3.068 ± 0.146	$5.680\times10^{-3}\pm1\times10^{-5}$	2.009 ± 0.023
$1.690\times10^{-2}\pm3\times10^{-5}$	3.190 ± 0.105	$5.010\times10^{-3}\pm1\times10^{-5}$	2.055 ± 0.012
$1.524\times10^{-2}\pm3\times10^{-5}$	3.186 ± 0.088	$4.351\times10^{-3}\pm1\times10^{-5}$	2.165 ± 0.012
$1.358\times10^{-2}\pm2\times10^{-5}$	3.304 ± 0.077	$3.696\times10^{-3}\pm1\times10^{-5}$	2.281 ± 0.008
$1.191\times10^{-2}\pm2\times10^{-5}$	3.455 ± 0.041	$3.031\times10^{-3}\pm1\times10^{-5}$	2.434 ± 0.055
$1.091\times10^{-2}\pm2\times10^{-5}$	3.642 ± 0.124	$2.701\times10^{-3}\pm1\times10^{-5}$	2.491 ± 0.009
$9.917\times10^{-3}\pm2\times10^{-5}$	3.718 ± 0.213	$2.368\times10^{-3}\pm1\times10^{-5}$	2.593 ± 0.007
$8.925\times10^{-3}\pm2\times10^{-5}$	3.912 ± 0.103	$2.032\times10^{-3}\pm1\times10^{-5}$	2.700 ± 0.006
$8.253\times10^{-3}\pm2\times10^{-5}$	3.985 ± 0.141	$1.701\times10^{-3}\pm1\times10^{-5}$	2.841 ± 0.011
$7.589\times10^{-3}\pm2\times10^{-5}$	4.153 ± 0.107	$1.371\times10^{-3}\pm1\times10^{-5}$	3.020 ± 0.014
$6.944\times10^{-3}\pm2\times10^{-5}$	4.014 ± 0.043	$1.039\times10^{-3}\pm1\times10^{-5}$	3.279 ± 0.014
$6.271\times10^{-3}\pm2\times10^{-5}$	4.199 ± 0.011	$9.259\times10^{-4}\pm2\times10^{-5}$	3.274 ± 0.012
$5.602\times10^{-3}\pm2\times10^{-5}$	4.313 ± 0.032	$8.388\times10^{-4}\pm1\times10^{-5}$	3.467 ± 0.012
$4.943\times10^{-3}\pm2\times10^{-5}$	4.492 ± 0.005	$7.481\times10^{-4}\pm1\times10^{-5}$	3.576 ± 0.011
$4.273\times10^{-3}\pm2\times10^{-5}$	4.691 ± 0.008	$7.105\times10^{-4}\pm1\times10^{-5}$	3.628 ± 0.009
$3.614\times10^{-3}\pm2\times10^{-5}$	4.812 ± 0.013	$6.504\times10^{-4}\pm1\times10^{-5}$	3.701 ± 0.007
$3.292\times10^{-3}\pm2\times10^{-5}$	4.893 ± 0.012	$6.088\times10^{-4}\pm1\times10^{-5}$	3.783 ± 0.009
$2.959\times10^{-3}\pm2\times10^{-5}$	5.030 ± 0.008	$5.620\times10^{-4}\pm1\times10^{-5}$	3.846 ± 0.008
$2.622\times10^{-3}\pm2\times10^{-5}$	5.248 ± 0.009	$4.537\times10^{-4}\pm1\times10^{-5}$	3.942 ± 0.033
$2.285\times10^{-3}\pm2\times10^{-5}$	5.506 ± 0.007	$3.745\times10^{-4}\pm1\times10^{-5}$	4.229 ± 0.007
$1.949\times10^{-3}\pm2\times10^{-5}$	5.718 ± 0.008	$3.534\times10^{-4}\pm1\times10^{-5}$	4.118 ± 0.013
$1.620\times10^{-3}\pm2\times10^{-5}$	6.003 ± 0.019	$2.627\times10^{-4}\pm2\times10^{-5}$	4.375 ± 0.019
$1.287\times10^{-3}\pm2\times10^{-5}$	6.365 ± 0.013	$1.739\times10^{-4}\pm1\times10^{-5}$	4.872 ± 0.010
$9.517\times10^{-4}\pm2\times10^{-5}$	6.760 ± 0.008	$1.699\times10^{-4}\pm1\times10^{-5}$	4.911 ± 0.008
$6.200\times10^{-4}\pm2\times10^{-5}$	7.192 ± 0.011	$1.142\times10^{-4}\pm1\times10^{-5}$	5.195 ± 0.037
$6.019\times10^{-4}\pm1\times10^{-5}$	7.232 ± 0.013	$8.117\times10^{-5}\pm1\times10^{-5}$	5.333 ± 0.007
$2.930\times10^{-4}\pm2\times10^{-5}$	7.455 ± 0.013	$8.117\times10^{-5}\pm1\times10^{-5}$	5.290 ± 0.019
$1.571\times10^{-4}\pm1\times10^{-5}$	7.134 ± 0.007	$5.610\times10^{-5}\pm1\times10^{-5}$	5.533 ± 0.016
$1.165\times10^{-4}\pm1\times10^{-5}$	6.686 ± 0.036	$4.191\times10^{-5}\pm1\times10^{-5}$	5.592 ± 0.020
$9.866\times10^{-5}\pm1\times10^{-5}$	6.743 ± 0.007	$3.766\times10^{-5}\pm1\times10^{-5}$	5.375 ± 0.017
$7.194\times10^{-5}\pm1\times10^{-5}$	6.512 ± 0.012	$2.763\times10^{-5}\pm1\times10^{-5}$	5.602 ± 0.007
$3.861\times10^{-5}\pm1\times10^{-5}$	6.214 ± 0.007	$8.280\times10^{-6}\pm1\times10^{-5}$	5.799 ± 0.015
$3.662\times10^{-5}\pm1\times10^{-5}$	6.155 ± 0.013		
$1.861\times10^{-5}\pm8\times10^{-6}$	5.896 ± 0.016		
$1.815\times10^{-5}\pm1\times10^{-5}$	5.988 ± 0.010		
$5.046\times10^{-6}\pm1\times10^{-5}$	5.837 ± 0.012		

in Tables IV, V, VI, and VII of this manuscript. The results are given in Table VIII. The error-weighted means [23] for the four mixtures are $\int P_+ = 1.90\pm0.08$, $\int P_- = 1.60\pm0.13$, and $R_{MA} = 1.12\pm0.06$, where the errors represent one standard deviation. In Ref. [8] we presented evidence that the fitting method determines $\int P_-$ from the two-phase data very accurately, while the fitted value for $\int P_+$ from the one-phase data and the result for R_{MA} are systematically low by 3–4%. As in Ref. [8] we add 3.3% to the $\int P_+$ value and 3.9% to the R_{MA} value to obtain $\int P_+ = 1.96\pm0.08$, $\int P_- = 1.60\pm0.13$, and $R_{MA} = 1.16\pm0.06$ as our best estimates of these quantities. These three values are within one standard deviation of the values reported in Ref. [8]. This is not surprising considering that the new ellipsometric data, measured with an improved thermostat, differed from the old data only near T_c, while the $\int P_\pm$ values were fitted to the data far from T_c.

IV. THE SURFACE VOLUME FRACTION $\varphi_L(0,t)$

In the analysis of model I, which was developed in Ref. [8] and described in Sec. III of the current manuscript, the surface layer was assumed to be pure L, $\varphi_L(0,t) = 1$. This

TABLE V. Ellipsometric data as a function of the reduced temperature for the critical liquid mixture isobutyric acid-water (IW).

t (one-phase region)	$10^3\overline{\rho}$	t (two-phase region)	$10^3\overline{\rho}$
$8.004\times10^{-2}\pm5\times10^{-5}$	0.512 ± 0.026	$2.515\times10^{-2}\pm5\times10^{-5}$	0.665 ± 0.006
$7.670\times10^{-2}\pm5\times10^{-5}$	0.503 ± 0.019	$2.353\times10^{-2}\pm5\times10^{-5}$	0.653 ± 0.006
$7.338\times10^{-2}\pm5\times10^{-5}$	0.496 ± 0.020	$2.179\times10^{-2}\pm5\times10^{-5}$	0.661 ± 0.007
$7.005\times10^{-2}\pm5\times10^{-5}$	0.470 ± 0.023	$2.019\times10^{-2}\pm5\times10^{-5}$	0.621 ± 0.009
$6.672\times10^{-2}\pm5\times10^{-5}$	0.474 ± 0.023	$1.846\times10^{-2}\pm5\times10^{-5}$	0.618 ± 0.019
$6.341\times10^{-2}\pm5\times10^{-5}$	0.459 ± 0.031	$1.683\times10^{-2}\pm5\times10^{-5}$	0.622 ± 0.008
$6.009\times10^{-2}\pm5\times10^{-5}$	0.393 ± 0.018	$1.511\times10^{-2}\pm5\times10^{-5}$	0.604 ± 0.005
$5.675\times10^{-2}\pm5\times10^{-5}$	0.412 ± 0.022	$1.348\times10^{-2}\pm5\times10^{-5}$	0.578 ± 0.006
$5.342\times10^{-2}\pm5\times10^{-5}$	0.396 ± 0.020	$1.176\times10^{-2}\pm5\times10^{-5}$	0.534 ± 0.009
$5.008\times10^{-2}\pm5\times10^{-5}$	0.366 ± 0.021	$1.013\times10^{-2}\pm5\times10^{-5}$	0.528 ± 0.011
$4.675\times10^{-2}\pm5\times10^{-5}$	0.388 ± 0.015	$1.009\times10^{-2}\pm5\times10^{-5}$	0.498 ± 0.017
$4.337\times10^{-2}\pm5\times10^{-5}$	0.312 ± 0.039	$9.422\times10^{-3}\pm5\times10^{-5}$	0.494 ± 0.013
$4.003\times10^{-2}\pm5\times10^{-5}$	0.315 ± 0.032	$8.764\times10^{-3}\pm5\times10^{-5}$	0.533 ± 0.009
$3.673\times10^{-2}\pm5\times10^{-5}$	0.299 ± 0.022	$8.091\times10^{-3}\pm5\times10^{-5}$	0.496 ± 0.010
$3.338\times10^{-2}\pm5\times10^{-5}$	0.262 ± 0.021	$7.422\times10^{-3}\pm5\times10^{-5}$	0.463 ± 0.008
$3.169\times10^{-2}\pm5\times10^{-5}$	0.221 ± 0.019	$6.784\times10^{-3}\pm5\times10^{-5}$	0.468 ± 0.008
$3.004\times10^{-2}\pm5\times10^{-5}$	0.212 ± 0.018	$6.755\times10^{-3}\pm5\times10^{-5}$	0.438 ± 0.010
$2.837\times10^{-2}\pm5\times10^{-5}$	0.222 ± 0.013	$6.072\times10^{-3}\pm5\times10^{-5}$	0.402 ± 0.014
$2.669\times10^{-2}\pm5\times10^{-5}$	0.161 ± 0.010	$5.404\times10^{-3}\pm5\times10^{-5}$	0.395 ± 0.010
$2.500\times10^{-2}\pm5\times10^{-5}$	0.102 ± 0.014	$4.739\times10^{-3}\pm5\times10^{-5}$	0.344 ± 0.010
$2.335\times10^{-2}\pm5\times10^{-5}$	0.121 ± 0.017	$4.070\times10^{-3}\pm5\times10^{-5}$	0.345 ± 0.009
$2.166\times10^{-2}\pm5\times10^{-5}$	0.045 ± 0.018	$3.432\times10^{-3}\pm5\times10^{-5}$	0.304 ± 0.008
$2.000\times10^{-2}\pm5\times10^{-5}$	0.047 ± 0.013	$3.403\times10^{-3}\pm5\times10^{-5}$	0.306 ± 0.010
$1.838\times10^{-2}\pm5\times10^{-5}$	-0.011 ± 0.013	$3.035\times10^{-3}\pm5\times10^{-5}$	0.248 ± 0.007
$1.665\times10^{-2}\pm5\times10^{-5}$	-0.041 ± 0.012	$2.700\times10^{-3}\pm5\times10^{-5}$	0.206 ± 0.009
$1.503\times10^{-2}\pm5\times10^{-5}$	-0.098 ± 0.021	$2.377\times10^{-3}\pm5\times10^{-5}$	0.174 ± 0.007
$1.332\times10^{-2}\pm5\times10^{-5}$	-0.134 ± 0.015	$2.032\times10^{-3}\pm5\times10^{-5}$	0.125 ± 0.010
$1.162\times10^{-2}\pm5\times10^{-5}$	-0.215 ± 0.018	$1.700\times10^{-3}\pm5\times10^{-5}$	0.078 ± 0.009
$9.967\times10^{-3}\pm5\times10^{-5}$	-0.290 ± 0.015	$1.631\times10^{-3}\pm8\times10^{-6}$	0.057 ± 0.010
$9.939\times10^{-3}\pm5\times10^{-5}$	-0.295 ± 0.010	$1.362\times10^{-3}\pm5\times10^{-5}$	0.001 ± 0.012
$9.264\times10^{-3}\pm5\times10^{-5}$	-0.335 ± 0.016	$1.315\times10^{-3}\pm8\times10^{-6}$	0.010 ± 0.006
$8.595\times10^{-3}\pm5\times10^{-5}$	-0.381 ± 0.013	$1.028\times10^{-3}\pm5\times10^{-5}$	-0.090 ± 0.011
$7.929\times10^{-3}\pm5\times10^{-5}$	-0.406 ± 0.017	$9.987\times10^{-4}\pm8\times10^{-6}$	-0.111 ± 0.006
$7.330\times10^{-3}\pm5\times10^{-5}$	-0.462 ± 0.016	$6.839\times10^{-4}\pm5\times10^{-5}$	-0.257 ± 0.011
$6.615\times10^{-3}\pm5\times10^{-5}$	-0.502 ± 0.016	$6.824\times10^{-4}\pm8\times10^{-6}$	-0.296 ± 0.018
$6.578\times10^{-3}\pm5\times10^{-5}$	-0.549 ± 0.023	$5.169\times10^{-4}\pm8\times10^{-6}$	-0.446 ± 0.010
$5.922\times10^{-3}\pm5\times10^{-5}$	-0.579 ± 0.015	$4.377\times10^{-4}\pm8\times10^{-6}$	-0.418 ± 0.009
$5.251\times10^{-3}\pm5\times10^{-5}$	-0.653 ± 0.010	$3.611\times10^{-4}\pm7\times10^{-6}$	-0.509 ± 0.012
$4.575\times10^{-3}\pm5\times10^{-5}$	-0.745 ± 0.021	$3.506\times10^{-4}\pm5\times10^{-5}$	-0.487 ± 0.014
$3.900\times10^{-3}\pm5\times10^{-5}$	-0.872 ± 0.010	$2.802\times10^{-4}\pm8\times10^{-6}$	-0.663 ± 0.007
$3.262\times10^{-3}\pm5\times10^{-5}$	-0.984 ± 0.012	$2.043\times10^{-4}\pm7\times10^{-6}$	-0.762 ± 0.010
$3.233\times10^{-3}\pm5\times10^{-5}$	-0.989 ± 0.011	$1.369\times10^{-4}\pm8\times10^{-6}$	-0.754 ± 0.010
$2.979\times10^{-3}\pm5\times10^{-5}$	-1.020 ± 0.013	$8.192\times10^{-5}\pm8\times10^{-6}$	-0.895 ± 0.007
$2.653\times10^{-3}\pm5\times10^{-5}$	-1.116 ± 0.033	$1.314\times10^{-5}\pm8\times10^{-6}$	-0.991 ± 0.006
$2.318\times10^{-3}\pm5\times10^{-5}$	-1.199 ± 0.018		
$1.988\times10^{-3}\pm5\times10^{-5}$	-1.304 ± 0.019		
$1.653\times10^{-3}\pm5\times10^{-5}$	-1.356 ± 0.016		
$1.652\times10^{-3}\pm6\times10^{-6}$	-1.403 ± 0.009		
$1.324\times10^{-3}\pm7\times10^{-6}$	-1.512 ± 0.014		
$1.316\times10^{-3}\pm5\times10^{-5}$	-1.492 ± 0.025		
$1.002\times10^{-3}\pm7\times10^{-6}$	-1.507 ± 0.013		
$9.767\times10^{-4}\pm5\times10^{-5}$	-1.576 ± 0.020		

TABLE V. (Continued).

$6.784\times10^{-4}\pm8\times10^{-6}$	-1.560 ± 0.021
$6.448\times10^{-4}\pm5\times10^{-5}$	-1.601 ± 0.031
$4.303\times10^{-4}\pm6\times10^{-6}$	-1.564 ± 0.104
$3.567\times10^{-4}\pm8\times10^{-6}$	-1.590 ± 0.016
$2.742\times10^{-4}\pm7\times10^{-6}$	-1.537 ± 0.008
$1.936\times10^{-4}\pm7\times10^{-6}$	-1.413 ± 0.006
$1.186\times10^{-4}\pm9\times10^{-6}$	-1.259 ± 0.015
$1.130\times10^{-4}\pm8\times10^{-6}$	-1.231 ± 0.012
$4.235\times10^{-5}\pm9\times10^{-6}$	-1.124 ± 0.010
$2.487\times10^{-5}\pm8\times10^{-6}$	-1.067 ± 0.007

assumption is plausible because for each mixture we have studied the liquid-vapor surface tension of pure H, σ_H, is considerably larger than the liquid-vapor surface tension of pure L, σ_L. However, no quantitative argument was offered in Ref. [8] to support this assumption. Franck and co-workers [24,25] have used optical reflectivity and capillary rise measurements to study critical adsorption of the nitromethane–carbon disulfide system at the liquid-solid surface, and have found the pure surface layer assumption to be invalid under certain circumstances. In fact, they discovered that a crossover from preferential adsorption of nitromethane to carbon disulfide occurs as the solid surface chemistry is varied from a hydroxylated to a methylated coverage. Previous papers that analyzed ellipsometry measurements of critical adsorption at the liquid-vapor surface effectively fixed the surface composition by proposing optical dielectric profiles on the liquid and vapor sides of the surface with relatively few adjustable parameters, and imposing the condition of continuity and smoothness of the profile at $z=0$ [19,26,27]. In this section we develop an estimate of the surface composition $\varphi_L(0,t)$ using a statistical mechanical theory and surface tension measurements.

The liquid-vapor surface tension of a critical binary liquid mixture was predicted by Ramos-Gomez and Widom [28] to have the reduced temperature dependence

$$\sigma_{\pm}(t)=\sigma_0+K_{\pm}t^{\mu}. \tag{22}$$

The term σ_0 is the analytic contribution of the noncritical profile, while $K_{\pm}t^{\mu}$ is the leading singular term contributed by the critical profile, with the critical exponent $\mu=2-\alpha-\nu\simeq1.26$. Fisher and Upton [29] used a local functional theory to derive a value for the ratio of the non-universal amplitudes $K_{\pm}$,

$$Q=\frac{K_+}{K_-}\simeq-0.83. \tag{23}$$

An experimental test of Eqs. (22) and (23) was provided by Privat and co-workers [30]. Their tensiometer measurements of the liquid-vapor surface tension of the critical mixture 2,5 lutidine-water were statistically fitted to Eq. (22), with σ_0 assumed to be linear in t, to obtain $\mu=1.21\pm0.09$ and $Q=-0.43\pm0.11$. With their fitted $K_{\pm}$ values, the critical term contributes only a few percent variation to σ within a range of $T_c\pm10$ °C. Our analysis below will use the approximation $\sigma\simeq\sigma_0$. This considers the contribution of the noncritical profile within a few molecular layers of the surface, where the density gradient is very large, but neglects the contribution of the slowly varying critical profile. The validity of this approximation is also suggested by the van der Waals relation between the surface tension and the order-parameter profile [21], $m(z,t)$,

$$\sigma\propto\int\left[\frac{dm(z,t)}{dz}\right]^2dz. \tag{24}$$

This mean-field result states that the largest contribution to σ originates from the steepest gradient in the order parameter profile, namely, from the noncritical profile at least for liquid-vapor surfaces.

A number of classical methods for estimating the noncritical contribution to the surface tension of liquid mixtures are summarized by Prausnitz, Sherwood, and Reid [31]. For aqueous solutions, or more generally for mixtures where the surface tension of one component is considerably larger than the other, the method of Tamura, Kurata, and Odani σ_0 is related to the surface volume fraction $\varphi_L(0,t)$ by the equation

$$\sigma_0^{1/4}=\varphi_L(0,t)\sigma_L^{1/4}+[1-\varphi_L(0,t)]\sigma_H^{1/4}. \tag{25}$$

The surface volume fraction is determined by the bulk volume fraction $\varphi_L(+\infty,t)$ and the surface tension difference $\sigma_H-\sigma_L$ through the relation

$$\frac{\varphi_L(0,t)}{1-\varphi_L(0,t)}=\frac{\varphi_L(+\infty,t)}{1-\varphi_L(+\infty,t)}\exp\left[\frac{\alpha(\sigma_H-\sigma_L)}{k_BT}\right]. \tag{26}$$

Here the parameter α is the area per molecule at the liquid-vapor surface of the mixture. Equations (25) and (26) are semiempirical, but bear strong resemblance to the results of Prigogine and Marechal [32] derived from the application of statistical mechanics to a lattice-gas model. In this theory the liquid-vapor surface is assumed to be one monolayer thick; that is, the bulk liquid and vapor phases are separated by a surface monolayer with a volume fraction of $\varphi_L(0,t)$. This approximation seems plausible for the noncritical profile.

One would expect α to be on the order of $v_L^{2/3}$ and $v_H^{2/3}$, where v_L and v_H are the molecular volumes in the bulk liquid of pure L and H, respectively. Since the surface layer should have a composition of nearly pure L, $\alpha\cong v_L^{2/3}$ should be a reasonable approximation. Tamura *et al.* tested Eq. (25) and variations of Eq. (26) with surface tension data for 16

TABLE VI. Ellipsometric data as a function of the reduced temperature for the critical liquid mixture 2,6 lutidine-water (LW).

t (one-phase region)	$10^3\overline{\rho}$	t (two-phase region)	$10^3\overline{\rho}$
$4.989\times10^{-2}\pm5\times10^{-5}$	-0.772 ± 0.047	$5.416\times10^{-2}\pm5\times10^{-5}$	0.551 ± 0.036
$4.346\times10^{-2}\pm5\times10^{-5}$	-0.768 ± 0.023	$4.768\times10^{-2}\pm5\times10^{-5}$	0.499 ± 0.029
$3.703\times10^{-2}\pm5\times10^{-5}$	-0.877 ± 0.032	$4.121\times10^{-2}\pm5\times10^{-5}$	0.480 ± 0.023
$3.058\times10^{-2}\pm5\times10^{-5}$	-1.044 ± 0.095	$3.475\times10^{-2}\pm5\times10^{-5}$	0.430 ± 0.024
$2.413\times10^{-2}\pm5\times10^{-5}$	-1.234 ± 0.049	$2.827\times10^{-2}\pm5\times10^{-5}$	0.482 ± 0.034
$2.091\times10^{-2}\pm5\times10^{-5}$	-1.342 ± 0.029	$2.500\times10^{-2}\pm5\times10^{-5}$	0.440 ± 0.034
$1.769\times10^{-2}\pm5\times10^{-5}$	-1.453 ± 0.021	$2.177\times10^{-2}\pm5\times10^{-5}$	0.263 ± 0.030
$1.447\times10^{-2}\pm5\times10^{-5}$	-1.657 ± 0.029	$1.853\times10^{-2}\pm5\times10^{-5}$	0.238 ± 0.028
$1.124\times10^{-2}\pm5\times10^{-5}$	-1.928 ± 0.031	$1.528\times10^{-2}\pm5\times10^{-5}$	0.208 ± 0.022
$8.023\times10^{-3}\pm5\times10^{-5}$	-2.292 ± 0.017	$1.204\times10^{-2}\pm5\times10^{-5}$	0.008 ± 0.085
$7.229\times10^{-3}\pm5\times10^{-5}$	-2.513 ± 0.019	$8.816\times10^{-3}\pm5\times10^{-5}$	-0.137 ± 0.018
$6.900\times10^{-3}\pm5\times10^{-5}$	-2.534 ± 0.019	$5.516\times10^{-3}\pm5\times10^{-5}$	-0.335 ± 0.014
$6.564\times10^{-3}\pm5\times10^{-5}$	-2.550 ± 0.020	$5.183\times10^{-3}\pm5\times10^{-5}$	-0.369 ± 0.013
$6.234\times10^{-3}\pm5\times10^{-5}$	-2.603 ± 0.025	$4.844\times10^{-3}\pm5\times10^{-5}$	-0.424 ± 0.014
$5.901\times10^{-3}\pm5\times10^{-5}$	-2.634 ± 0.019	$4.821\times10^{-3}\pm5\times10^{-5}$	-0.444 ± 0.024
$5.571\times10^{-3}\pm5\times10^{-5}$	-2.671 ± 0.013	$4.527\times10^{-3}\pm5\times10^{-5}$	-0.462 ± 0.013
$5.255\times10^{-3}\pm5\times10^{-5}$	-2.758 ± 0.024	$4.191\times10^{-3}\pm5\times10^{-5}$	-0.511 ± 0.020
$4.932\times10^{-3}\pm5\times10^{-5}$	-2.878 ± 0.019	$3.871\times10^{-3}\pm5\times10^{-5}$	-0.571 ± 0.016
$4.798\times10^{-3}\pm5\times10^{-5}$	-2.951 ± 0.032	$3.551\times10^{-3}\pm5\times10^{-5}$	-0.631 ± 0.015
$4.596\times10^{-3}\pm5\times10^{-5}$	-2.955 ± 0.023	$3.225\times10^{-3}\pm5\times10^{-5}$	-0.713 ± 0.019
$4.269\times10^{-3}\pm5\times10^{-5}$	-3.071 ± 0.018	$2.898\times10^{-3}\pm5\times10^{-5}$	-0.792 ± 0.020
$3.939\times10^{-3}\pm5\times10^{-5}$	-3.174 ± 0.014	$2.572\times10^{-3}\pm5\times10^{-5}$	-0.876 ± 0.021
$3.613\times10^{-3}\pm5\times10^{-5}$	-3.273 ± 0.015	$2.242\times10^{-3}\pm5\times10^{-5}$	-0.961 ± 0.019
$3.287\times10^{-3}\pm5\times10^{-5}$	-3.386 ± 0.017	$1.968\times10^{-3}\pm1\times10^{-5}$	-1.012 ± 0.019
$2.964\times10^{-3}\pm5\times10^{-5}$	-3.559 ± 0.015	$1.909\times10^{-3}\pm5\times10^{-5}$	-1.055 ± 0.019
$2.640\times10^{-3}\pm5\times10^{-5}$	-3.722 ± 0.017	$1.740\times10^{-3}\pm1\times10^{-5}$	-1.116 ± 0.021
$2.311\times10^{-3}\pm5\times10^{-5}$	-3.919 ± 0.015	$1.593\times10^{-3}\pm5\times10^{-5}$	-1.123 ± 0.013
$1.981\times10^{-3}\pm5\times10^{-5}$	-4.114 ± 0.018	$1.586\times10^{-3}\pm5\times10^{-5}$	-1.217 ± 0.018
$1.655\times10^{-3}\pm5\times10^{-5}$	-4.384 ± 0.015	$1.505\times10^{-3}\pm1\times10^{-5}$	-1.193 ± 0.014
$1.576\times10^{-3}\pm5\times10^{-5}$	-4.593 ± 0.052	$1.297\times10^{-3}\pm7\times10^{-6}$	-1.294 ± 0.017
$1.532\times10^{-3}\pm5\times10^{-6}$	-4.638 ± 0.014	$1.257\times10^{-3}\pm5\times10^{-5}$	-1.406 ± 0.022
$1.322\times10^{-3}\pm5\times10^{-5}$	-4.701 ± 0.012	$1.079\times10^{-3}\pm7\times10^{-6}$	-1.466 ± 0.017
$1.207\times10^{-3}\pm5\times10^{-6}$	-4.927 ± 0.067	$9.928\times10^{-4}\pm4\times10^{-5}$	-1.457 ± 0.008
$1.005\times10^{-3}\pm5\times10^{-5}$	-5.037 ± 0.020	$8.464\times10^{-4}\pm7\times10^{-6}$	-1.667 ± 0.035
$9.067\times10^{-4}\pm2\times10^{-5}$	-5.288 ± 0.014	$7.746\times10^{-4}\pm3\times10^{-5}$	-1.656 ± 0.011
$6.756\times10^{-4}\pm5\times10^{-5}$	-5.520 ± 0.027	$7.414\times10^{-4}\pm3\times10^{-6}$	-1.688 ± 0.023
$5.434\times10^{-4}\pm3\times10^{-6}$	-5.589 ± 0.023	$6.237\times10^{-4}\pm2\times10^{-6}$	-1.866 ± 0.022
$4.514\times10^{-4}\pm2\times10^{-6}$	-6.012 ± 0.013	$5.599\times10^{-4}\pm3\times10^{-5}$	-1.927 ± 0.013
$3.648\times10^{-4}\pm3\times10^{-6}$	-6.059 ± 0.008	$5.174\times10^{-4}\pm3\times10^{-6}$	-2.053 ± 0.010
$2.787\times10^{-4}\pm5\times10^{-6}$	-6.047 ± 0.014	$4.098\times10^{-4}\pm4\times10^{-6}$	-2.275 ± 0.017
$1.924\times10^{-4}\pm8\times10^{-6}$	-5.998 ± 0.065	$3.146\times10^{-4}\pm3\times10^{-6}$	-2.412 ± 0.007
$1.536\times10^{-4}\pm6\times10^{-6}$	-5.876 ± 0.012	$2.826\times10^{-4}\pm6\times10^{-6}$	-2.503 ± 0.013
$1.469\times10^{-4}\pm4\times10^{-6}$	-5.978 ± 0.031	$2.358\times10^{-4}\pm4\times10^{-6}$	-2.721 ± 0.006
$1.219\times10^{-4}\pm8\times10^{-6}$	-5.853 ± 0.027	$1.995\times10^{-4}\pm5\times10^{-6}$	-2.867 ± 0.009
$1.154\times10^{-4}\pm7\times10^{-6}$	-5.856 ± 0.012	$1.511\times10^{-4}\pm5\times10^{-6}$	-3.006 ± 0.012
$9.417\times10^{-5}\pm1\times10^{-5}$	-5.362 ± 0.044	$1.079\times10^{-4}\pm5\times10^{-6}$	-3.256 ± 0.016
$7.741\times10^{-5}\pm9\times10^{-6}$	-4.686 ± 0.017	$5.753\times10^{-5}\pm5\times10^{-6}$	-3.518 ± 0.014
$5.433\times10^{-5}\pm6\times10^{-6}$	-4.489 ± 0.040	$3.605\times10^{-5}\pm9\times10^{-6}$	-3.594 ± 0.014
$3.408\times10^{-5}\pm1\times10^{-5}$	-4.199 ± 0.010	$1.624\times10^{-5}\pm5\times10^{-6}$	-3.629 ± 0.013
$1.949\times10^{-5}\pm1\times10^{-6}$	-4.020 ± 0.029	$9.967\times10^{-6}\pm9\times10^{-6}$	-3.740 ± 0.005
$1.059\times10^{-5}\pm1\times10^{-5}$	-3.907 ± 0.009		

TABLE VII. Ellipsometric data as a function of the reduced temperature for the critical liquid mixture nitrobenzene-hexane (NH).

t (one-phase region)	$10^3\overline{\rho}$	t (two-phase region)	$10^3\overline{\rho}$
$8.480\times10^{-2}\pm5\times10^{-5}$	2.519 ± 0.014	$2.207\times10^{-2}\pm5\times10^{-5}$	1.565 ± 0.012
$6.775\times10^{-2}\pm5\times10^{-5}$	2.686 ± 0.015	$2.038\times10^{-2}\pm5\times10^{-5}$	1.583 ± 0.018
$5.082\times10^{-2}\pm5\times10^{-5}$	2.864 ± 0.016	$1.869\times10^{-2}\pm5\times10^{-5}$	1.637 ± 0.015
$3.410\times10^{-2}\pm5\times10^{-5}$	2.957 ± 0.031	$1.700\times10^{-2}\pm5\times10^{-5}$	1.685 ± 0.020
$3.388\times10^{-2}\pm5\times10^{-5}$	3.147 ± 0.010	$1.530\times10^{-2}\pm5\times10^{-5}$	1.725 ± 0.016
$3.068\times10^{-2}\pm5\times10^{-5}$	3.153 ± 0.008	$1.386\times10^{-2}\pm5\times10^{-5}$	1.787 ± 0.008
$2.723\times10^{-2}\pm5\times10^{-5}$	3.242 ± 0.008	$1.361\times10^{-2}\pm5\times10^{-5}$	1.774 ± 0.015
$2.380\times10^{-2}\pm5\times10^{-5}$	3.365 ± 0.006	$1.192\times10^{-2}\pm5\times10^{-5}$	1.846 ± 0.014
$2.044\times10^{-2}\pm5\times10^{-5}$	3.501 ± 0.006	$1.120\times10^{-2}\pm5\times10^{-5}$	1.913 ± 0.008
$1.702\times10^{-2}\pm5\times10^{-5}$	3.666 ± 0.008	$1.022\times10^{-2}\pm5\times10^{-5}$	1.924 ± 0.016
$1.691\times10^{-2}\pm5\times10^{-5}$	3.739 ± 0.017	$8.522\times10^{-3}\pm5\times10^{-5}$	2.024 ± 0.017
$1.364\times10^{-2}\pm5\times10^{-5}$	3.751 ± 0.007	$7.564\times10^{-3}\pm5\times10^{-5}$	2.125 ± 0.006
$1.026\times10^{-2}\pm5\times10^{-5}$	4.251 ± 0.006	$6.830\times10^{-3}\pm5\times10^{-5}$	2.099 ± 0.013
$1.023\times10^{-2}\pm5\times10^{-5}$	4.067 ± 0.018	$5.790\times10^{-3}\pm5\times10^{-5}$	2.569 ± 0.007
$9.918\times10^{-3}\pm5\times10^{-5}$	4.280 ± 0.005	$5.141\times10^{-3}\pm5\times10^{-5}$	2.452 ± 0.018
$9.580\times10^{-3}\pm5\times10^{-5}$	4.328 ± 0.004	$5.131\times10^{-3}\pm5\times10^{-5}$	2.295 ± 0.014
$9.239\times10^{-3}\pm5\times10^{-5}$	4.379 ± 0.007	$3.439\times10^{-3}\pm5\times10^{-5}$	2.570 ± 0.018
$8.901\times10^{-3}\pm5\times10^{-5}$	4.406 ± 0.022	$3.231\times10^{-3}\pm5\times10^{-5}$	2.571 ± 0.011
$8.556\times10^{-3}\pm5\times10^{-5}$	4.325 ± 0.057	$3.013\times10^{-3}\pm5\times10^{-5}$	2.760 ± 0.010
$8.219\times10^{-3}\pm5\times10^{-5}$	4.373 ± 0.008	$2.675\times10^{-3}\pm5\times10^{-5}$	2.904 ± 0.009
$7.881\times10^{-3}\pm5\times10^{-5}$	4.529 ± 0.048	$2.334\times10^{-3}\pm5\times10^{-5}$	3.044 ± 0.016
$7.536\times10^{-3}\pm5\times10^{-5}$	4.598 ± 0.007	$2.003\times10^{-3}\pm5\times10^{-5}$	3.016 ± 0.011
$7.199\times10^{-3}\pm5\times10^{-5}$	4.657 ± 0.006	$1.658\times10^{-3}\pm5\times10^{-5}$	3.144 ± 0.013
$6.854\times10^{-3}\pm5\times10^{-5}$	4.737 ± 0.008	$1.433\times10^{-3}\pm3\times10^{-5}$	3.225 ± 0.007
$6.786\times10^{-3}\pm5\times10^{-5}$	4.684 ± 0.009	$1.307\times10^{-3}\pm5\times10^{-5}$	3.477 ± 0.016
$6.513\times10^{-3}\pm5\times10^{-5}$	4.850 ± 0.013	$9.621\times10^{-4}\pm5\times10^{-5}$	3.721 ± 0.014
$6.168\times10^{-3}\pm5\times10^{-5}$	4.734 ± 0.177	$8.870\times10^{-4}\pm5\times10^{-5}$	3.572 ± 0.015
$5.817\times10^{-3}\pm5\times10^{-5}$	4.764 ± 0.006	$8.256\times10^{-4}\pm5\times10^{-5}$	3.626 ± 0.013
$5.465\times10^{-3}\pm5\times10^{-5}$	4.888 ± 0.076	$7.676\times10^{-4}\pm5\times10^{-5}$	3.701 ± 0.011
$5.128\times10^{-3}\pm5\times10^{-5}$	5.141 ± 0.009	$7.096\times10^{-4}\pm5\times10^{-5}$	3.774 ± 0.015
$4.797\times10^{-3}\pm5\times10^{-5}$	5.223 ± 0.016	$6.791\times10^{-4}\pm1\times10^{-5}$	3.885 ± 0.012
$4.459\times10^{-3}\pm5\times10^{-5}$	5.307 ± 0.009	$6.482\times10^{-4}\pm5\times10^{-5}$	3.836 ± 0.017
$4.125\times10^{-3}\pm5\times10^{-5}$	5.425 ± 0.013	$6.209\times10^{-4}\pm5\times10^{-5}$	4.039 ± 0.012
$3.784\times10^{-3}\pm5\times10^{-5}$	5.312 ± 0.143	$5.902\times10^{-4}\pm5\times10^{-5}$	3.922 ± 0.012
$3.456\times10^{-3}\pm5\times10^{-5}$	5.382 ± 0.014	$5.288\times10^{-4}\pm5\times10^{-5}$	4.001 ± 0.013
$3.112\times10^{-3}\pm5\times10^{-5}$	5.522 ± 0.063	$4.708\times10^{-4}\pm5\times10^{-5}$	4.118 ± 0.020
$3.089\times10^{-3}\pm7\times10^{-5}$	5.636 ± 0.014	$4.060\times10^{-4}\pm5\times10^{-5}$	4.230 ± 0.014
$2.777\times10^{-3}\pm5\times10^{-5}$	5.797 ± 0.032	$3.480\times10^{-4}\pm5\times10^{-5}$	4.362 ± 0.021
$2.487\times10^{-3}\pm5\times10^{-5}$	5.853 ± 0.012	$2.832\times10^{-4}\pm5\times10^{-5}$	4.732 ± 0.010
$2.439\times10^{-3}\pm5\times10^{-5}$	5.974 ± 0.006	$2.798\times10^{-4}\pm5\times10^{-5}$	4.495 ± 0.012
$2.098\times10^{-3}\pm5\times10^{-5}$	6.150 ± 0.007	$2.286\times10^{-4}\pm5\times10^{-5}$	4.676 ± 0.012
$1.882\times10^{-3}\pm4\times10^{-5}$	6.228 ± 0.022	$1.706\times10^{-4}\pm5\times10^{-5}$	4.880 ± 0.013
$1.757\times10^{-3}\pm5\times10^{-5}$	6.368 ± 0.005	$1.241\times10^{-4}\pm1\times10^{-5}$	5.059 ± 0.007
$1.423\times10^{-3}\pm5\times10^{-5}$	6.463 ± 0.104	$1.058\times10^{-4}\pm5\times10^{-5}$	5.124 ± 0.016
$1.304\times10^{-3}\pm3\times10^{-5}$	6.416 ± 0.014	$6.943\times10^{-5}\pm2\times10^{-5}$	5.222 ± 0.007
$1.075\times10^{-3}\pm5\times10^{-5}$	6.702 ± 0.017	$5.620\times10^{-5}\pm2\times10^{-5}$	5.297 ± 0.008
$9.177\times10^{-4}\pm5\times10^{-5}$	7.009 ± 0.013	$4.435\times10^{-5}\pm5\times10^{-5}$	5.365 ± 0.014
$8.563\times10^{-4}\pm5\times10^{-5}$	7.021 ± 0.021	$3.494\times10^{-5}\pm2\times10^{-5}$	5.264 ± 0.006
$7.168\times10^{-4}\pm2\times10^{-5}$	7.116 ± 0.021	$9.785\times10^{-6}\pm2\times10^{-5}$	5.369 ± 0.016
$6.020\times10^{-4}\pm2\times10^{-5}$	7.154 ± 0.011	$4.953\times10^{-6}\pm2\times10^{-5}$	5.483 ± 0.016
$5.343\times10^{-4}\pm2\times10^{-5}$	7.327 ± 0.024		
$4.811\times10^{-4}\pm2\times10^{-5}$	7.329 ± 0.106		
$3.514\times10^{-4}\pm2\times10^{-5}$	7.334 ± 0.014		

TABLE VII. (Continued).

$3.042\times10^{-4}\pm1\times10^{-5}$	7.259 ± 0.040
$2.512\times10^{-4}\pm1\times10^{-5}$	7.084 ± 0.049
$1.932\times10^{-4}\pm2\times10^{-5}$	7.009 ± 0.008
$1.476\times10^{-4}\pm2\times10^{-5}$	6.994 ± 0.016
$1.092\times10^{-4}\pm2\times10^{-5}$	6.526 ± 0.014
$1.008\times10^{-4}\pm1\times10^{-5}$	6.451 ± 0.019
$8.001\times10^{-5}\pm1\times10^{-5}$	6.425 ± 0.015
$6.391\times10^{-5}\pm1\times10^{-5}$	6.032 ± 0.024
$5.775\times10^{-5}\pm1\times10^{-5}$	6.084 ± 0.005
$1.689\times10^{-5}\pm2\times10^{-5}$	5.532 ± 0.031

different liquid mixtures and found the error to be less than 10% over a wide range of concentrations for most of the mixtures. None of these mixtures was near their liquid-liquid critical point. The applicability of formulas similar to Eqs. (25) and (26) in the vicinity of the liquid-liquid critical point was tested by Ramakrishna and Patel [33] with the surface tension data of several mixtures. Their conclusion, stated in terms of Eqs. (25) and (26), was that the theoretical formulas did not agree well with the surface tension data when $\alpha=v_L^{2/3}$ was used, but fitting α as an adjustable parameter gave good agreement.

Figure 1 shows the surface tension of the mixture IW at the critical composition as a function of the reduced temperature for both the one-phase and two-phase regions. The closed circles represent the surface light-scattering measurements of Nagarajan, Webb, and Widom [34] in the one-phase region. The open squares and open triangles represent the capillary-rise measurements of Khosla and Widom [35] in the one-phase and two-phase regions, respectively. The solid and dashed lines represent Eqs. (25) and (26) in the one-phase and two-phase regions, respectively, and differ from the experimental data by a fraction of a percent in the one-phase region and by less than 3% in the two-phase region. To obtain this high level of agreement the surface area per molecule α in Eq. (26) was decreased by only 2.4% from its estimated value of $(v_L)^{2/3}=2.87\times10^{-15}$ cm^2 to the value $\alpha=2.73\times10^{-15}$ cm^2.

Liquid-vapor surface tension measurements are also avail-

TABLE VIII. Nonlinear least-squares fit of Eqs. (17), (18), (20), and (21) (referred to as model I) to ellipsometric data far from T_c. (Quoted errors are one standard deviation.)

Mixture	Phase	Reduced temperature range	$\beta-\nu$ [a]	Fitted $10^3\overline{\rho}_{\text{pure}}$	Measured $10^3\overline{\rho}_{\text{pure}}$ [b]	$\int P_{\pm}$	R_{MA} [c]	χ^2
AC	1	$0.004<t<0.04$	-0.306 ± 0.011	1.22 ± 0.08	1.09 ± 0.05 (C)	2.12 ± 0.22	1.08 ± 0.03	2.6
AC	1	$0.004<t<0.04$	-0.304	1.20 ± 0.04	(1.22 ± 0.05)[d]	2.14 ± 0.13		2.4
AC	2	$0.0008<t<0.04$	-0.303 ± 0.013	0.98 ± 0.09		2.01 ± 0.27		0.35
AC	2	$0.0008<t<0.04$	-0.304	0.99 ± 0.04		1.98 ± 0.12		0.33
IW	1	$0.007<t$	-0.303 ± 0.022	1.46 ± 0.14	0.90 ± 0.05 (I)	2.06 ± 0.34	1.55 ± 0.09	0.12
IW	1	$0.007<t$	-0.304	1.45 ± 0.06		2.04 ± 0.12		0.11
IW	2	$0.0015<t$	-0.312 ± 0.039	0.88 ± 0.10		1.24 ± 0.43		0.11
IW	2	$0.0015<t$	-0.304	0.90 ± 0.04		1.32 ± 0.10		0.11
LW	1	$0.004<t$	-0.306 ± 0.011	1.10 ± 0.22	1.06 ± 0.05 (L)	1.79 ± 0.17	1.19 ± 0.02	0.74
LW	1	$0.004<t$	-0.304	1.13 ± 0.10		1.81 ± 0.10		0.70
LW	2	$0.0008<t$	-0.290 ± 0.011	1.11 ± 0.08		1.69 ± 0.16		0.90
LW	2	$0.0008<t$	-0.304	1.02 ± 0.04		1.52 ± 0.08		0.90
NH	1	$0.005<t$	-0.308 ± 0.009	1.41 ± 0.06	1.03 ± 0.05 (H)	1.74 ± 0.14	1.02 ± 0.02	2.5
NH	1	$0.005<t$	-0.304	1.39 ± 0.03		1.79 ± 0.09		2.4
NH	2	$0.001<t$	-0.297 ± 0.012	0.94 ± 0.08		1.87 ± 0.21		3.3
NH	2	$0.001<t$	-0.304	0.98 ± 0.03		1.76 ± 0.10		3.2

[a]The value of -0.304 implies that $\beta-\nu$ has been fixed at this value.

[b]From Ref. [8], measured at room temperature, unless otherwise noted. (C) indicates that the value was measured on pure cyclohexane, (I) indicates isobutyric acid, etc. These are the components that are preferentially adsorbed at the surface.

[c]Calculated from the one- and two-phase fitted values of $\int P_{\pm}$ with $\beta-\nu$ fixed.

[d]From Ref. [27], at $T=25\,^{\circ}$C.

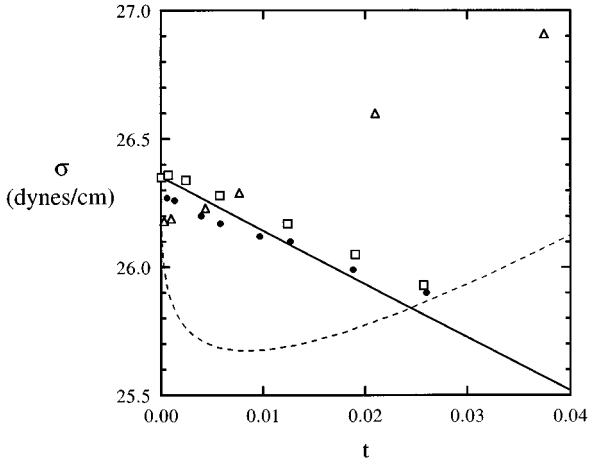

FIG. 1. Liquid-vapor surface tension σ of the critical liquid mixture IW as a function of the reduced temperature t. The solid and dashed lines represent Eqs. (25) and (26) in the one-phase and the two-phase regions, respectively. The open squares and open triangles represent the capillary-rise measurements of Khosla and Widom [35] in the one-phase and the two-phase regions, respectively. The surface light scattering measurements of Nagarajan, Webb, and Widom [34] taken in the one-phase region are represented by the closed circles. The agreement between the theory and the experimental data is not as good in the two-phase region, but is still better than 3%.

able for the mixtures AC [33,36], LW [37], and NH [33,38]. These measurements were taken as a function of composition at a few temperatures in the one-phase region. From these data the value for σ at the critical composition at each temperature could be determined by linear interpolation.

In Table IX the liquid-vapor surface tensions for pure L and H, σ_L and σ_H, are given for each mixture along with the surface area per molecule, α, and the calculated values for $v_L^{2/3}$ and $v_H^{2/3}$. As discussed above for the mixture IW, the given values of α were determined by comparing Eqs. (25) and (26) with the available surface tension data. The approximation $\alpha \simeq v_L^{2/3}$ is only accurate for the mixture IW. With the values of α given in Table IX, the surface tension values derived from Eqs. (25) and (26) always differ from the experimental values by less than 5%. For the purpose of this paper it appears that Eqs. (25) and (26), with α determined by surface tension measurements, provide a satisfactory estimate of $\varphi_L(0,t)$ and σ. It should be emphasized, however, that this assertion has been tested in the two-phase region for IW only.

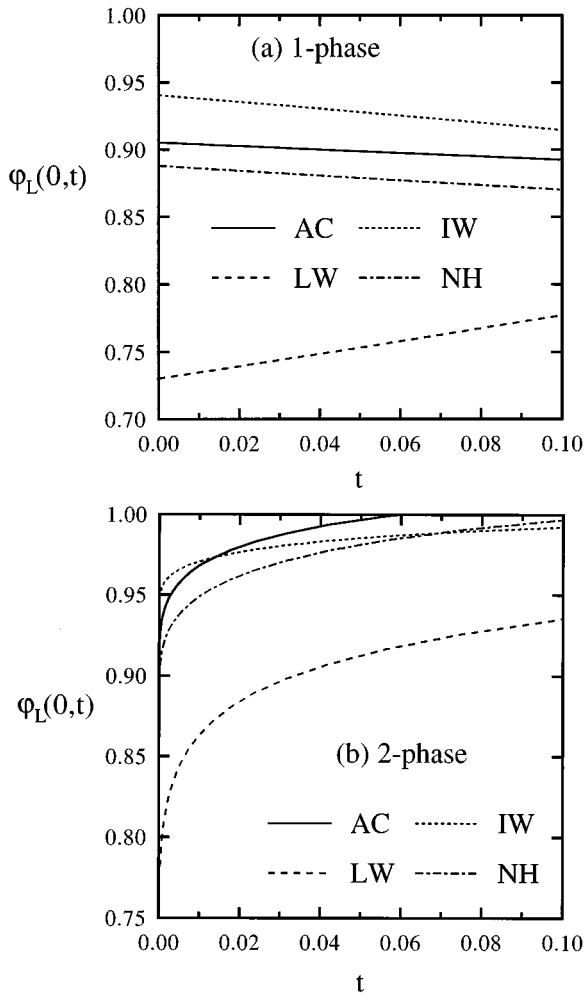

FIG. 2. Volume fraction of component L at $z=0$, $\varphi_L(0,t)$, as a function of the reduced temperature t, calculated using Eq. (26). Curves are shown for all four mixtures (a) in the one-phase region, and (b) in the two-phase region. The approximation $\varphi_L(0,t)=1$ appears to be particularly invalid for the mixture LW.

In Figs. 2(a) and 2(b) the surface volume fraction determined from Eq. (26) is graphed as a function of the reduced temperature t for all four mixtures in the one-phase and two-

TABLE IX. The first two columns provide the liquid-vapor surface tensions for pure L and H, where T is the temperature in degrees Celsius. The third column states the surface area per molecule of the liquid mixture, determined by comparing Eqs. (25) and (26) with the measured values of σ as described in the text. For comparison, the surface area per molecule of pure L and H should be approximately equal to the values provided in the final two columns.

Mixture	σ_L [a] (dyne/cm)	σ_H [a] (dyne/cm)	α (10^{-15} cm^2)	$(v_L)^{2/3}$ (10^{-15} cm^2)	$(v_H)^{2/3}$ (10^{-15} cm^2)
AC	$27.62-0.1188T$	$44.83-0.1085T$	4.50	3.14	2.84
IW	$26.88-0.0920T$	$75.83-0.1477T$	2.73	2.87	0.96
LW	$33.91-0.1159T$	$75.83-0.1477T$	1.90	3.35	0.96
NH	$20.44-0.1022T$	$46.34-0.1157T$	2.50	3.61	3.07

[a]Reference [59].

phase regions, respectively. At least for the mixture LW it appears that $\varphi_L(0,t)=1$ is not a good approximation.

Once $\varphi_L(0,t)$ is determined, $\epsilon(0,t)$ and z_e can be determined as a function of t from Eqs. (8) and (16). However, if $z_e \ll \xi_\pm$ does not hold then the analytic Eq. (16) is not valid, and z_e must be determined numerically using Eqs. (1) and (2) at $z=0$.

V. CAPILLARY WAVES

Superimposed on the static intrinsic profile at the liquid-vapor surface are thermally generated surface oscillations called capillary waves. Their presence at the critical liquid-liquid interface in the two-phase region, where the surface tension approaches zero as t approaches zero, has been shown to be crucial to the interpretation of ellipsometric measurements on this surface [12,39–41]. The contribution of capillary waves at the noncritical liquid-vapor surface was neglected in model I (see Sec. III) and most previous publications on critical adsorption with the exception of two recent papers by Findenegg and co-workers [26,42]. The surface tension at the liquid-vapor surface does not approach zero as t approaches zero, so the amplitudes of the capillary wave oscillations remain finite, and the contribution to $\overline{\rho}$ should remain small. In this section we address the question of whether or not this contribution is actually negligible.

Marvin and Toiga [43] have shown that for light reflecting off a surface for which both the thickness of the static intrinsic profile and the amplitudes of the capillary wave oscillations are small compared to the wavelength of light λ, the contributions of the capillary waves and the intrinsic profile to $\overline{\rho}$ are additive. Thus the ellipsometric measurement on the liquid-vapor surface of a liquid mixture can be written as

$$\overline{\rho}=\overline{\rho_{\rm cw}}+\overline{\rho_{\rm ip}}, \tag{27}$$

where $\overline{\rho_{\rm cw}}$ is the capillary wave contribution and $\overline{\rho_{\rm ip}}$ is the intrinsic profile contribution discussed in Sec. III. For the case of capillary waves roughening a surface with its intrinsic profile width approaching zero, capillary wave theory has been used to predict $\overline{\rho_{\rm cw}}$ [12,39]. This result applied to the liquid-vapor surface of the liquid mixture is

$$\overline{\rho_{\rm cw}}=\frac{3}{4\lambda}\frac{\epsilon(+\infty,t)-1}{\sqrt{\epsilon(+\infty,t)+1}}\frac{k_BT}{\sigma}q_m, \tag{28}$$

where q_m is the maximum wave number of the capillary wave oscillations. Buff, Lovett, and Stillinger [9] postulated that

$$q_m=\frac{a}{\xi_v}, \tag{29}$$

where the parameter a is approximately 0.75 [44]. For this result it is the noncritical profile for which the thickness approaches zero, while the influence of the critical profile on $\overline{\rho_{\rm cw}}$ is neglected entirely. Meunier [45] developed the alternative form

$$q_m=\frac{\pi}{2}\sqrt{\frac{\sigma}{k_c}}, \tag{30}$$

where k_c is the rigidity constant of the liquid-vapor surface of the mixture. If Eq. (30) were to be used, k_c would need to be treated as an adjustable parameter. Equation (29) adds no new adjustable parameters, since the noncritical correlation length ξ_v has already been included in the noncritical profile in Eq. (14). For this reason if Eq. (29) proves to be accurate, it would be preferable to Eq. (30).

Recently Kuzmin and Romanov [41] have derived $\overline{\rho_{\rm cw}}$ for the case of capillary waves roughening a Fisk-Widom intrinsic profile with a non-negligible thickness, as opposed to the infinitesimal profile thickness considered in Refs. [12,39]. Their result is an expansion in $\Delta\epsilon$, the difference in the bulk optical dielectric constants on either side of the surface. They found their result to be in better agreement with the ellipsometric measurements of Schmidt [40] on the critical interface of binary liquid mixtures near T_c compared with Eqs. (28) and (29). However, their result is not applicable to the liquid-vapor surface in our experiment, where $\Delta\epsilon$ is large. Equation (28) does not assume that $\Delta\epsilon$ is small and is therefore more relevant for our situation.

The right-hand side of Eq. (28) contains only factors that do not diverge as $t\to 0$, so that $\overline{\rho_{\rm cw}}$ merely provides another background term to $\overline{\rho}$, with a weak, nondiverging dependence on t. We therefore rewrite Eqs. (27), (17), and (18) as

$$\overline{\rho}=\overline{\rho_{\rm bg}}-\frac{\pi}{\lambda}f_\epsilon(t)(\eta_L-\eta_H)M_-\xi_{0\pm}(\textstyle\int P_\pm)t^{\beta-\nu}, \tag{31}$$

where

$$\begin{aligned}\overline{\rho_{\rm bg}}&=\overline{\rho_{\rm cw}}+\overline{\rho_{\rm bg,ip}}\\&=\overline{\rho_{\rm cw}}+\overline{\rho_{\rm nc}}-\frac{\pi}{\lambda}f_\epsilon(t)(\eta_L-\eta_H)M_-\xi_{0\pm}[I_1(t)+I_2(t)].\end{aligned} \tag{32}$$

To calculate $\overline{\rho_{\rm cw}}$ from Eq. (28), ξ_v must be determined, along with k_c if Eq. (30) is used rather than Eq. (29). In Sec. VI the $(\overline{\rho},t)$ data of each mixture are statistically fitted to Eqs. (31) and (32), and ξ_v (or ξ_v and k_c) is determined as a fitting parameter for each mixture in the one-phase and two-phase regions. Using these ξ_v and k_c values in Eqs. (28), (29), and (30), $\overline{\rho_{\rm cw}}$ is plotted as a function of t for the mixture IW in Fig. 3. The curve labeled ''1'' was calculated using Eq. (29), while the curve labeled ''2'' was calculated using Eq. (30). The variation of $\overline{\rho_{\rm cw}}$ with t is on the order of 10^{-4} for both curve 1 and 2. This is small compared to the variation of $\overline{\rho}$, which is on the order of 5×10^{-3}, but is not negligible since the uncertainty in the measured $\overline{\rho}$ values is on the order of 10^{-5}. For curve 1, $\overline{\rho_{\rm cw}}$ is proportional to σ^{-1}, while $\overline{\rho_{\rm cw}}$ is proportional to $\sigma^{-1/2}$ for curve 2. This provides curve 1 with the stronger dependence on t. Figure 3 also shows that the difference between $\overline{\rho_{\rm cw}}$ in curve 1 and curve 2 is approximately 3×10^{-4}. This large difference is due to the fact that for curve 2 both ξ_v and k_c were fitted as adjustable parameters. In Eq. (32), k_c determines the value of $\overline{\rho_{\rm cw}}$ and ξ_v determines the value of $\overline{\rho_{\rm nc}}$. Since $\overline{\rho_{\rm bg}}$, $\overline{\rho_{\rm cw}}$, and $\overline{\rho_{\rm nc}}$ are all

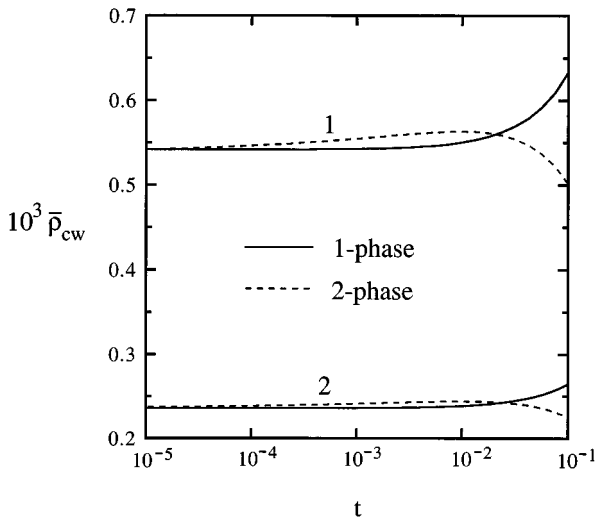

FIG. 3. Semilogarithmic plot of the capillary wave contribution to $\overline{\rho}$, times 1000, as a function of the reduced temperature t. Both the one-phase (solid lines) and two-phase (dashed lines) curves are shown for the mixture IW. The curves labeled ''1'' were calculated using Eqs. (28) and (29), while the curves labeled ''2'' were calculated using Eqs. (28) and (30).

nearly constant, the statistical fit determines $\overline{\rho_{bg}}$ precisely, but determines $\overline{\rho_{cw}}$ and $\overline{\rho_{nc}}$ very imprecisely.

VI. RESULTS AND DISCUSSION

In Ref. [8] and Sec. III the $(\overline{\rho},t)$ data far from T_c were statistically fitted to Eqs. (17), (18), (20), and (21), which we call model I in the current manuscript. Model I neglects the capillary wave contribution $\overline{\rho_{cw}}$ and assumes that the surface layer consists of pure L, $\varphi_L(0,t)=1$. The pure surface layer assumption led to the further assumption that the noncritical profile of the liquid mixture is identical to the liquid-vapor profile of pure L. This allowed $\overline{\rho_{nc}}$ to be expressed in terms of $\overline{\rho_{pure}}$ in Eq. (20) with ξ_v in Eq. (21) being determined by the measured value of $\overline{\rho_{pure}}$. The fitting parameters in model I include $\overline{\rho_{pure}}$, and its fitted value can be compared to the measured value as an additional test of the model's accuracy. The fitted results for $\overline{\rho_{pure}}$, $\int P_+$, and $\int P_-$ are listed in Table VIII.

In Secs. IV and V a model to describe the $(\overline{\rho},t)$ data far from T_c is presented, and is summarized by Eqs. (31) and (32). The assumption $\varphi_L(0,t)=1$ is eliminated with the determination of $\varphi_L(0,t)$ in Eq. (26). Equations (20) and (21) are no longer valid for this situation, and therefore Eq. (19) will be used to determine $\overline{\rho_{nc}}$, and ξ_v will be fitted rather than $\overline{\rho_{pure}}$. The capillary wave contribution to $\overline{\rho}$ is approximated by $\overline{\rho_{cw}}$ in Eq. (28), with q_m being determined by either Eq. (29) or Eq. (30). This model will be referred to as models II(a) and II(b) when Eqs. (29) and (30) are used, respectively. For model II(b), k_c must be fitted as an additional adjustable parameter, which makes model II(a) more desirable if it proves to be accurate.

The results of a nonlinear least-squares regression fit [23] of the $(\overline{\rho},t)$ data to model II(a) are presented in Table X. Initially $\beta-\nu$ was fitted along with ξ_v and $\int P_\pm$ to verify the critical scaling, then ξ_v and $\int P_\pm$ were fitted with $\beta-\nu=-0.304$ fixed at the theoretical value in order to increase the precision of the fitted $\int P_\pm$ values.

TABLE X. Nonlinear least-squares fit of Eqs. (19), (28), (29), (31), and (32) [referred to as model II(a)] to ellipsometric data far from T_c. (Quoted errors are one standard deviation.)

Mixture	Phase	Reduced temperature range	$\beta-\nu$ [a]	ξ_v (Å)	$\int P_\pm$	R_{MA} [b]	χ^2
AC	1	$0.004<t<0.04$	-0.306 ± 0.002	1.39 ± 0.75	1.97 ± 0.11	1.32 ± 0.008	3.9
AC	1	$0.004<t<0.04$	-0.304	1.32 ± 0.08	2.00 ± 0.12		3.9
AC	2	$0.0008<t<0.04$	-0.306 ± 0.0009	1.21 ± 0.06	1.50 ± 0.09		8.4
AC	2	$0.0008<t<0.04$	-0.304	1.18 ± 0.05	1.51 ± 0.09		8.2
IW	1	$0.007<t$	-0.304 ± 0.001	1.28 ± 0.016	2.02 ± 0.11	1.00 ± 0.009	0.43
IW	1	$0.007<t$	-0.304	1.28 ± 0.07	2.01 ± 0.10		0.52
IW	2	$0.0015<t$	-0.300 ± 0.001	1.16 ± 0.04	2.02 ± 0.11		3.7
IW	2	$0.0015<t$	-0.304	1.29 ± 0.07	2.01 ± 0.11		3.6
LW	1	$0.004<t$	-0.300 ± 0.0005	0.87 ± 0.05	2.10 ± 0.11	1.08 ± 0.004	3.4
LW	1	$0.004<t$	-0.304	0.84 ± 0.05	2.05 ± 0.10		4.1
LW	2	$0.0008<t$	-0.294 ± 0.0005	1.01 ± 0.02	1.95 ± 0.10		8.8
LW	2	$0.0008<t$	-0.304	1.25 ± 0.04	1.90 ± 0.10		9.8
NH	1	$0.005<t$	-0.308 ± 0.017	1.00 ± 0.23	1.82 ± 0.22	1.33 ± 0.01	2.1
NH	1	$0.005<t$	-0.304	1.06 ± 0.07	1.87 ± 0.10		2.1
NH	2	$0.001<t$	-0.306 ± 0.0008	1.46 ± 0.10	1.40 ± 0.07		11.1
NH	2	$0.001<t$	-0.304	1.39 ± 0.09	1.41 ± 0.07		10.8

[a]The value of -0.304 implies that $\beta-\nu$ has been fitted at this value.

[b]Calculated from the one- and two-phase fitted values of $\int P_\pm$ with $\beta-\nu$ fixed.

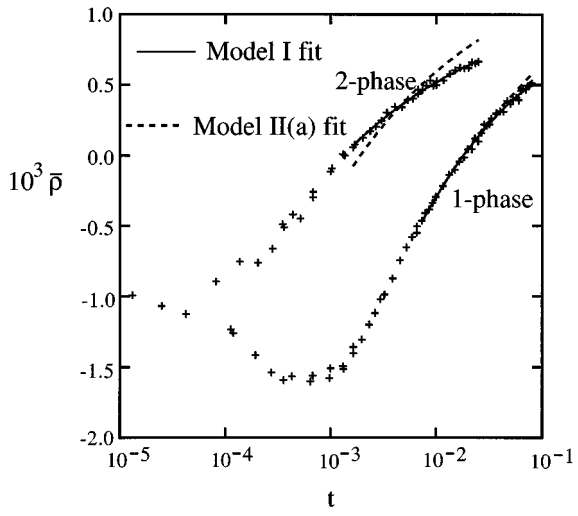

FIG. 4. Semilogarithmic plot of the coefficient of ellipticity $\overline{\rho}$, times 1000, for the critical liquid mixture IW in both the one-phase and two-phase regions, as a function of the reduced temperature t. The experimental data are represented by plusses, while the fitted functions of models I and II(a) are represented by the solid and dashed lines, respectively. The poor agreement of the model II(a) with the experimental data is evident in the two-phase region over the entire fitted range, and in the one-phase region for large t.

A comparison of model I (Table VIII) and model II(a) (Table X) for the one-phase region shows mostly modest changes in the fitting results. Except for the mixture LW, the changes in the fitted $\int P_+$ values are well under 10%. The fitted $\beta-\nu$ values are all more or less unchanged and in good agreement with the theoretical value of -0.304. The reduced chi-squared values χ^2 have only changed slightly for the mixtures AC and NH, but have increased by approximately a factor of five for IW and LW, which indicates that the quality of the fit has been reduced significantly. The two-phase region results of model II(a) differ more dramatically from the model I results. For all four mixtures the fitted $\int P_-$ values have changed by more than 20% and the χ^2 values have increased by an order of magnitude. This indicates that the model II(a) fitting function is unable to provide a t dependence that matches the data well in the two-phase region and therefore the two-phase results in Table X are suspect. The increase in the χ^2 values from Table VIII to Table X is largest for the mixture IW. Figure 4 shows the $(\overline{\rho},t)$ data for this mixture in both the one-phase and two-phase regions with the fitted functions of models I and II(a) represented by the solid and dashed lines, respectively. The solid lines follow the data well over the entire range of the one-phase and two-phase fitted intervals of t. The dashed line, however, begins to deviate at large reduced temperatures in the one-phase region, and fits the data poorly at all reduced temperatures in the two-phase region.

In order to isolate the source of the poor agreement between model II(a) and the experimental data in the two-phase region, the data were refitted to this model function with $\overline{\rho}_{\rm cw}$ removed from Eq. (32). This fit, which will be called model III, is identical to model I except that $\varphi_L(0,t)$ is determined by Eq. (26) rather than by the assumption $\varphi_L(0,t)=1$. The results are provided in Table XI. The χ^2

TABLE XI. Nonlinear least-squares fit of ellipsometric data far from T_c to Eqs. (19), (31), and (32), with $\overline{\rho}_{\rm cw}=0$ imposed (referred to as model III). (Quoted errors are one standard deviation.)

Mixture	Phase	Reduced temperature range	$\beta-\nu$ [a]	ξ_ν (Å)	$\int P_\pm$	R_{MA} [b]	χ^2
AC	1	$0.004<t<0.04$	-0.307 ± 0.011	2.24 ± 0.21	2.10 ± 0.22	1.06 ± 0.03	2.5
AC	1	$0.004<t<0.04$	-0.304	2.19 ± 0.11	2.14 ± 0.13		2.4
AC	2	$0.0008<t<0.04$	-0.301 ± 0.013	1.52 ± 0.17	2.06 ± 0.27		0.36
AC	2	$0.0008<t<0.04$	-0.304	1.55 ± 0.08	2.01 ± 0.12		0.34
IW	1	$0.007<t$	-0.301 ± 0.022	2.72 ± 0.29	2.07 ± 0.34	1.49 ± 0.09	0.12
IW	1	$0.007<t$	-0.304	2.69 ± 0.11	2.03 ± 0.12		0.11
IW	2	$0.0015<t$	-0.311 ± 0.037	1.71 ± 0.22	1.29 ± 0.44		0.11
IW	2	$0.0015<t$	-0.304	1.75 ± 0.10	1.36 ± 0.10		0.11
LW	1	$0.004<t$	-0.308 ± 0.069	1.03 ± 1.0	1.79 ± 0.97	1.10 ± 0.02	0.70
LW	1	$0.004<t$	-0.304	1.09 ± 0.08	1.84 ± 0.10		0.66
LW	2	$0.0008<t$	-0.290 ± 0.010	1.77 ± 0.14	1.88 ± 0.18		1.1
LW	2	$0.0008<t$	-0.304	1.60 ± 0.06	1.67 ± 0.09		1.1
NH	1	$0.005<t$	-0.307 ± 0.009	3.63 ± 0.21	1.70 ± 0.14	0.96 ± 0.02	2.5
NH	1	$0.005<t$	-0.304	3.56 ± 0.10	1.74 ± 0.09		2.4
NH	2	$0.001<t$	-0.292 ± 0.012	1.62 ± 0.18	2.00 ± 0.21		3.5
NH	2	$0.001<t$	-0.304	1.79 ± 0.07	1.82 ± 0.10		3.3

[a]The value of -0.304 implies that $\beta-\nu$ has been fixed at this value.

[b]Calculated from the one- and two-phase fitted values of $\int P_\pm$ with $\beta-\nu$ fixed.

TABLE XII. Nonlinear least-squares fit of Eqs. (19), (28), (30), (31), and (32) [referred to as model II(b)] to ellipsometric data far from T_c. (Quoted errors are one standard deviation.)

Mixture	Phase	Reduced temperature range	$\beta-\nu$ [a]	k_c (10^{-14} dyne cm)	ξ_v (Å)	$\int P_{\pm}$	R_{MA} [b]	χ^2
AC	1	$0.004<t<0.04$	-0.308 ± 0.010	6 ± 5	1.5 ± 1	2.10 ± 0.22	1.09 ± 0.03	2.5
AC	1	$0.004<t<0.04$	-0.304	6 ± 5	1.4 ± 1	2.17 ± 0.13		2.3
AC	2	$0.0008<t<0.04$	-0.301 ± 0.013	10 ± 8	1.0 ± 0.5	2.05 ± 0.27		0.35
AC	2	$0.0008<t<0.04$	-0.304	10 ± 8	1.1 ± 0.5	1.99 ± 0.12		0.33
IW	1	$0.007<t$	-0.301 ± 0.023	10 ± 6	2.0 ± 0.8	2.02 ± 0.34	1.47 ± 0.09	0.11
IW	1	$0.007<t$	-0.304	10 ± 6	1.9 ± 0.8	1.98 ± 0.12		0.10
IW	2	$0.0015<t$	-0.307 ± 0.036	10 ± 8	1.2 ± 0.5	1.32 ± 0.44		0.11
IW	2	$0.0015<t$	-0.304	10 ± 8	1.2 ± 0.5	1.35 ± 0.10		0.10
LW	1	$0.004<t$	-0.308 ± 0.055	14 ± 10	0.8 ± 0.2	1.78 ± 0.76	1.17 ± 0.09	0.70
LW	1	$0.004<t$	-0.304	14 ± 10	0.8 ± 0.2	1.84 ± 0.10		0.66
LW	2	$0.0008<t$	-0.293 ± 0.011	3 ± 2	0.8 ± 0.4	1.72 ± 0.18		0.93
LW	2	$0.0008<t$	-0.304	3 ± 2	0.7 ± 0.4	1.57 ± 0.08		0.93
NH	1	$0.005<t$	-0.307 ± 0.008	5 ± 3	2.5 ± 0.4	1.76 ± 0.15	1.00 ± 0.02	2.3
NH	1	$0.005<t$	-0.304	5 ± 3	2.4 ± 0.4	1.80 ± 0.09		2.3
NH	2	$0.001<t$	-0.292 ± 0.012	5 ± 4	0.9 ± 0.4	1.98 ± 0.21		3.4
NH	2	$0.001<t$	-0.304	5 ± 4	1.0 ± 0.4	1.80 ± 0.10		3.3

[a]The value of -0.304 implies that $\beta-\nu$ has been fitted at this value.
[b]Calculated from the one- and two-phase fitted values of $\int P_{\pm}$ with $\beta-\nu$ fixed.

values are nearly identical in Tables VIII and XI, and the changes in the fitted $\int P_{\pm}$ values are all on the order of or less than one standard deviation. The conclusion that seems evident from this is that the capillary wave contribution $\overline{\rho_{\rm cw}}$ in Eq. (28), with q_m determined by Eq. (29), is in poor agreement with the experimental data in the two-phase region. It is also in poor agreement in the one-phase region for the mixtures IW and LW.

The results of fitting the $(\overline{\rho},t)$ data using model II(b), where q_m is determined by Eq. (30), are listed in Table XII. The values of $\beta-\nu$, $\int P_{\pm}$, and χ^2 in Table XII are nearly identical to the corresponding values in Tables VIII and XI, which indicates that the data have been fitted quite accurately in Table XII. Thus the poor quality fit in Table X is due solely to Eq. (29), and replacing Eq. (29) with Eq. (30) provides an accurate fit to the experimental data. The unfortunate side of this is that Eq. (30) adds k_c as a second adjustable parameter in the nearly constant background term $\overline{\rho_{\rm bg}}$. Because of this, k_c and ξ_v, the other adjustable parameters in $\overline{\rho_{\rm bg}}$, are both very poorly determined, as can be seen by their large uncertainties in Table XII. It is important to note, however, that when Eq. (29) is used, the model is in poor agreement with the experimental data regardless of the value of ξ_v. When Eq. (30) is used, on the other hand, the model is in very good agreement with the data over a large range of values of ξ_v and k_c.

For each of the three successful fits in this paper [models I, II(b), and III], the experimental error-weighted means [23] of the four mixtures' values of $\int P_{\pm}$ and R_{MA} are stated with one-standard deviation errors in Table XIII. In Ref. [8] we presented evidence that this type of fitting method determines $\int P_{+}$ and R_{MA} values, which are on average 3–4% low. The numbers in parentheses in Table XIII have been given a 3.3% correction for $\int P_{+}$ and a 3.9% correction for R_{MA}. The appropriate correction is not known exactly, but the corrected values in parentheses should be more accurate than the uncorrected values.

The $\overline{\rho}(t)$ functions of models I, II(b), and III differ only in their functional forms of the background term $\overline{\rho_{\rm bg}}$, which is nearly independent of t. The critical term, proportional to $(\int P_{\pm})t^{\beta-\nu}$, is identical for the three model functions. Although the formulation of $\overline{\rho_{\rm bg}}$ has weaknesses in all three of the models, we have no reason to believe that the form of the critical term, from which the $\int P_{\pm}$ and $\beta-\nu$ values are fitted, contains any significant error. This is supported by the fact that the fitted values for the exponent $\beta-\nu$ from all three of the models are in good agreement with the theoretical value. Despite the three different forms for $\overline{\rho_{\rm bg}}$, the mean values of $\int P_{\pm}$ given in the experimental rows of Table XIII have a very small spread. This lends credibility to the accuracy of these experimental mean values and to the small uncertainties which are stated for them.

At least one physical effect that could have contributed to the measured $\overline{\rho}$ values has not been included in our model. This is the effect of any anisotropy in the dielectric constant that may exist near the liquid-vapor surface. It has been shown that anisotropy can provide an important contribution to ellipsometric measurements [46]. It is caused by a net alignment of the electric dipoles of the molecules, and is expected to occur only within a few molecular layers of the surface. Thus it should affect the noncritical profile only, so that it would merely provide another nearly constant contri-

TABLE XIII. Comparison of the existing theoretical values for the universal critical adsorption parameters $\int P_{\pm}$, R_{MA}, and R_{Φ} with the experimental values obtained in this paper and in the literature. Our experimental values are the error-weighted means of the values fitted for the four mixtures in Tables VIII (model I), XI (model III), and XII [model II(b)]. The values in parentheses have been adjusted in an effort to account for small systematic errors. See text for details.

		$\int P_{+}$	$\int P_{-}$	R_{MA}	R_{Φ}
Theory	RG[a]	1.91	1.44	1.33	2.61
	MC[b]	2.18	1.97	1.11	2.18
	I[c]	2.27 ± 0.33	1.84 ± 0.33	1.32 ± 0.07	2.28 ± 0.10
Experiment	Model I	$1.90(1.96)\pm0.08$	1.60 ± 0.13	$1.12(1.16)\pm0.06$	$2.20(2.29)\pm0.12$
	Model III	$1.89(1.95)\pm0.09$	1.69 ± 0.13	$1.04(1.08)\pm0.05$	$2.04(2.12)\pm0.10$
	Model II(b)	$1.91(1.97)\pm0.08$	1.65 ± 0.13	$1.09(1.13)\pm0.05$	$2.13(2.21)\pm0.10$
	Flöter and Dietrich[c]	2.5 ± 0.5	2.53		

[a]Reference [3].
[b]Reference [4].
[c]Reference [7].

bution to $\overline{\rho_{\mathrm{bg}}}$. As Table XIII demonstrates, neglecting contributions to ρ_{bg} provides negligible error to the fitted $\int P_{\pm}$ and $\beta-\nu$ values. We suggest that if anisotropy actually had a strong influence on the critical profile, then the fitted values of $\beta-\nu$ would not be in good agreement with the theoretical value.

Flöter and Dietrich [7] have extracted a surface scaling function $P_{+}(x)$ from each of the adsorption profiles determined from the ellipsometry experiments of Findenegg and coworkers [42,47] and from the reanalysis of optical data by Liu and Fisher [19]. These experimental functions scatter widely relative to one another and relative to the theoretical functions, particularly in the crossover region $x\sim1$ between the two asymptotic limits. This could be due to the fact that the profiles were all formulated with multiple adjustable parameters. From these experimental profiles Flöter and Dietrich obtained the estimate $g_{+}\simeq0.75\pm0.15$, where the amplitude relation $\int P_{\pm}=g_{\pm}/(\nu-\beta)$ gives $\int P_{+}\simeq2.5\pm0.5$. This estimate is the mean value obtained from seven different mixtures, and an uncertainty of one standard deviation has been supplied. Flöter and Dietrich were also able to extract the two-phase function $P_{-}(x)$ from the ellipsometric data on the liquid-vapor surface of a critical liquid mixture measured by Hirtz, Lawnik, and Findenegg [47], from which they obtained $g_{-}\simeq0.768$, which gives $\int P_{-}\simeq2.53$. This value is from one mixture only, and its uncertainty could not be estimated. These estimates of $\int P_{\pm}$ are included in the experimental section of Table XIII.

The available theoretical values for the universal numbers $\int P_{\pm}$ and R_{MA} are also provided in Table XIII, where RG refers to the renormalization-group study of Diehl and Smock [3], MC refers to the Monte Carlo study of Smock, Diehl, and Landau [4], and I refers to the interpolation study of Flöter and Dietrich [7]. The three theories have a much smaller spread in their values for the one-phase result $\int P_{+}$ than for the two-phase result $\int P_{-}$. Our experimental values suggest that all three of the theoretical estimates of $\int P_{+}$ are reasonably accurate. Our fitted experimental values of $\int P_{-}$ are approximately halfway between the RG and I values.

Possible sources of systematic error to our experimental values of $\int P_{\pm}$ are the measured values of the nonuniversal parameters listed in Tables II, III, and IX. Of particular concern is the correlation length amplitude ξ_{0+}, since the fitted experimental values of $\int P_{+}$ and $\int P_{-}$ are inversely proportional to the measured values of $\xi_{0\pm}$ used in Eq. (31). This source of uncertainty has been propagated into the uncertainties stated for $\int P_{\pm}$ in Tables VIII, X, and XI. It is an important source of error because the uncertainty on the measurement of ξ_{0+} is typically on the order of 10%, and is even greater for ξ_{0-}, which is determined from the ξ_{0+} value using the approximate result of Eq. (15). Since the ratio R_{MA} is independent of the value used for ξ_{0+}, an incorrectly measured ξ_{0+} value would result in both the $\int P_{+}$ and $\int P_{-}$ values being either too high or too low, but the R_{MA} value would remain correct. While the experimental R_{MA} values are inversely proportional to the value used for the ratio ξ_{0+}/ξ_{0-}, Flöter and Dietrich [7] have pointed out that the quantity $R_{\Phi}=(\xi_{0+}/\xi_{0-})R_{MA}$ is independent of even this ratio. With the exception of the value from the interpolation study, all values of R_{Φ} listed in Table XIII were determined by multiplying the corresponding R_{MA} value by $\xi_{0+}/\xi_{0-}=1.96$ [22]. In the interpolation study [7] it was deduced that $\xi_{0+}/\xi_{0-}=1.73\pm0.04$ and $R_{\Phi}=2.28\pm0.10$. The value of R_{MA} given for this study in Table XIII was calculated from these two values. The experimental values of R_{Φ} in Table XIII are in good agreement with the theoretical values from the interpolation and MC studies.

VII. SUMMARY

We have presented our most accurate ellipsometric critical adsorption data, measured on the liquid-vapor surface of the critical mixtures AC, IW, LW, and NH. The Drude equation (7) was used to analyze the $(\overline{\rho},t)$ data far from T_c and provide an experimental estimate of the universal integrals $\int P_{\pm}$ defined in Eqs. (5a) and (5b).

Four variations on this analysis, which differed only in their treatment of the various nearly constant background contributions to $\overline{\rho}$, were applied to the data. In model I the uppermost surface layer of the liquid was assumed to be composed purely of the preferentially adsorbed component, and capillary wave fluctuations were ignored. In model III

the composition of the uppermost surface layer of the liquid was determined from liquid-vapor surface tension measurements for each mixture [Eqs. (25) and (26)] and again capillary wave fluctuations were ignored. In models II(a) and II(b) the surface layer composition was determined from surface tension measurements while the contribution due to the capillary wave fluctuations was approximated by Eqs. (28), with q_m determined by Eqs. (29) and (30), respectively. The results from these four methods of analysis are provided in Tables VIII, XI, X, and XII, respectively. While models I, II(b), and III provide very accurate descriptions of the experimental data, model II(a) fails to do so. The models I, II(b), and III results show that ellipsometry alone is insufficient to critically explore the nature of the background contributions. However, model II(a) provides an example in which ellipsometry does have sufficient sensitivity to discriminate against an inappropriately modeled background. The values of $\int P_{\pm}$ fitted from models I, II(b), and III are nearly identical (Table XIII). This is evidence that very accurate values for $\int P_{\pm}$ can be fitted to the ellipsometric data without a quantitatively accurate understanding of each of the background contributions.

We conclude that $\int P_{+} = 1.97 \pm 0.08$ and $\int P_{-} = 1.65 \pm 0.13$ [from the model II(b) fit] are our best experimental estimates of the universal integrals. Both of these experimental values lie within the range of the corresponding theoretical values available in the literature (Table XIII). However, the spreads in the theoretical values for $\int P_{+}$ and $\int P_{-}$ are many times greater than the uncertainties of the measured values.

ACKNOWLEDGMENTS

We wish to thank Professor M. Privat for supplying surface tension data for the mixture 2,6 lutidine–water. We also thank Professor H. W. Diehl, M. Smock, and Professor D. P. Landau for supplying numerical values and asymptotic forms for the theoretical surface scaling functions from the renormalization-group study and the Monte Carlo simulation. Finally, we thank Professor C. Franck and N. Desai for helpful discussions. This work was supported by the National Science Foundation through Grants No. DMR-9208123 and No. DMR-9500827.

[1] P. Kumar, Phys. Rev. B **10**, 2928 (1974); T. C. Lubensky and M. H. Ruben, *ibid.* **12**, 3885 (1975); K. Binder, in *Phase Transition and Critical Phenomena*, edited by C. Domb and J. L. Lebowitz (Academic, London, 1983), Vol. VIII, p. 1; H. W. Diehl, in *Phase Transitions and Critical Phenomena*, edited by C. Domb and J. L. Lebowitz (Academic, London, 1986), Vol. X, p. 75; K. Ohno and Y. Okabe, Phys. Rev. B **39**, 9764 (1989).

[2] M. E. Fisher and P.-G. de Gennes, C. R. Acad. Sci. Paris B **287**, 207 (1978).

[3] H. W. Diehl and M. Smock, Phys. Rev. B **47**, 5841 (1993); **48**, 6470(E) (1993).

[4] M. Smock, H. W. Diehl, and D. P. Landau, Ber. Bunsenges. Phys. Chem. **98**, 486 (1994). The RG values that we are using for C_{+}, C_{-}, and $P_{\infty,+}$ were obtained from Diehl and Smock through private correspondence, and differ somewhat from the values given in this publication.

[5] D. S. P. Smith, B. M. Law, M. Smock, and D. P. Landau (unpublished).

[6] D. P. Landau and K. Binder, Phys. Rev. B **41**, 4786 (1990).

[7] G. Flöter and S. Dietrich, Z. Phys. B **97**, 213 (1995).

[8] D. S. P. Smith and B. M. Law, Phys. Rev. E **52**, 580 (1995). The value of 0.502 given for $\varphi_L(+\infty,0)$ for IW in Table II of this paper was incorrect. The actual value was 0.392.

[9] F. P. Buff, R. A. Lovett, and F. H. Stillinger, Jr., Phys. Rev. Lett. **15**, 621 (1965).

[10] M. Tamura, M. Kurata, and H. Odani, Bull. Chem. Soc. Jpn. **28**, 83 (1955).

[11] D. Beaglehole, in *Fluid Interfacial Phenomena*, edited by C. A. Croxton (Wiley, New York, 1986).

[12] D. Beaglehole, Physica (Amsterdam) B **100**, 163 (1980).

[13] B. M. Law, Phys. Rev. Lett. **67**, 1555 (1991).

[14] D. S. P. Smith and B. M. Law, J. Chem. Phys. **99**, 9836 (1993).

[15] Beaglehole Instruments Ltd., 127 Kelburn Rd., Wellington, New Zealand.

[16] YSI Inc., Yellow Springs, OH 45387; product no. 44034. We have found that from a half dozen YSI 44034 thermistors of the same serial number, one can usually find two that have temperature-resistance curves matched to better than a few mK over a wide temperature range.

[17] P. K. L. Drude, *The Theory of Optics* (Dover, New York, 1959), p. 292.

[18] M. Born and E. Wolf, *Principles of Optics* (Pergamon, Oxford, 1980), Sec. 1.6; B. M. Law and D. Beaglehole, J. Phys. D **14**, 115 (1981); B. M. Law, Ph.D. thesis, Dept. of Physics, Victoria University of Wellington, New Zealand, 1985 (unpublished).

[19] A. J. Liu and M. E. Fisher, Phys. Rev. A **40**, 7202 (1989).

[20] W. V. Andrew, T. B. K. Khoo, and D. T. Jacobs, J. Chem. Phys. **85**, 3985 (1986).

[21] J. S. Rowlinson and B. Widom, *Molecular Theory of Capillarity* (Clarendon, Oxford, 1982).

[22] E. Brezin, J. C. Le Guillou, and J. Zinn-Justin, Phys. Lett. A **47**, 285 (1974); H. B. Tarko and M. E. Fisher, Phys. Rev. Lett. **31**, 926 (1973); A. J. Liu and M. E. Fisher, Physica (Amsterdam) A **156**, 35 (1989).

[23] P. R. Bevington, *Data Reduction and Error Analysis for the Physical Sciences* (McGraw-Hill, New York, 1969). Subroutine CURFIT of Chap. 11 is used for the nonlinear least-squares fit. The procedure used to calculate the error-weighted mean and standard deviation is from the bottom of p. 73.

[24] M. Schlossman, X.-L. Wu, and C. Franck, Phys. Rev. B **31**, 1478 (1985); J. Dixon, M. Schlossman, X.-L. Wu, C. Franck, *ibid.* **31**, 1509 (1985); C. Franck, J. Chem. Phys. **82**, 5633 (1985).

[25] N. S. Desai, S. Peach, and C. Franck, Phys. Rev. E **52**, 4129 (1995).

[26] R. Süssmann and G. H. Findenegg, Physica (Amsterdam) A **156**, 114 (1989).
[27] J. W. Schmidt, Phys. Rev. A **41**, 885 (1990).
[28] F. Ramos-Gomez and B. Widom, Physica A (Amsterdam) **104**, 595 (1980).
[29] M. E. Fisher and P. J. Upton, Phys. Rev. Lett. **65**, 2402 (1990); **65**, 3405 (1990).
[30] M. Amara, M. Privat, R. Bennes, and E. Tronel-Peyroz, J. Chem. Phys. **98**, 5028 (1993); S. Karad, M. Amara, A. Laouenan, E. Tronel-Peyroz, R. Bennes, and M. Privat, J. Chem. Phys. **100**, 1498 (1994).
[31] J. M. Prausnitz, T. K. Sherwood, and R. C. Reid, *The Properties of Gases and Liquids*, 3rd ed. (McGraw-Hill, New York, 1977), Chap. 12.
[32] I. Prigogine and J. Marechal, J. Colloid. Sci. **7**, 122 (1952).
[33] V. Ramakrishna and M. Patel, Indian J. Chem. **8**, 256 (1970).
[34] N. Nagarajan, W. W. Webb, and B. Widom, J. Chem. Phys. **77**, 5771 (1982).
[35] M. P. Khosla and B. Widom, J. Colloid Interface Sci. **76**, 375 (1980).
[36] J. Timmermans, *The Physico-Chemical Constants of Binary Systems in Concentrated Solutions* (Interscience Publishers, New York, 1959), Vol. I, p. 539.
[37] M. Privat, L. Tenebre, R. Bennes, E. Tronel-Peyroz, J. M. Douillard, and L. Ghaicha, Langmuir **4**, 1151 (1988); M. Privat (private correspondence).
[38] A. I. Rusanov, S. A. Levichev, and O. N. Mikhalenko, Russ. J. Phys. Chem. **43**, 1481 (1969).
[39] B. J. A. Zielinska, D. Bedeaux, and J. Vlieger, Physica A **107**, 91 (1981).
[40] J. W. Schmidt, Phys. Rev. A **38**, 567 (1988); Physica A **172**, 40 (1991); D. G. Miles, Jr., and J. W. Schmidt, J. Chem. Phys. **92**, 3881 (1990).
[41] V. L. Kuzmin and V. P. Romanov, Phys. Rev. E **49**, 2949 (1994).
[42] A. Hirtz, K. Bonkhoff, and G. H. Findenegg, Adv. Colloid Interface Sci. **44**, 241 (1993).
[43] A. M. Marvin and F. Toigo, Phys. Rev. A **26**, 2927 (1982).
[44] J. V. Sengers and J. M. J. Van Leeuwen, Phys. Rev A **39**, 6346 (1989); J. V. Sengers, J. M. J. Van Leeuwen, and J. W. Schmidt, Physica A **172**, 20 (1991).
[45] J. Meunier, J. Phys. (Paris) **48**, 1819 (1987).
[46] B. M. Law, J. Colloid Interface Sci. **134**, 1 (1990).
[47] A. Hirtz, W. Lawnik, and G. H. Findenegg, Colloids Surf. **51**, 405 (1990).
[48] P. Calmettes, I. Lagues, and C. Laj, Phys. Rev. Lett. **28**, 478 (1972).
[49] S. C. Greer, Phys. Rev. A **14**, 1770 (1976).
[50] Y. Jayalakshmi, J. S. Van Duijneveldt, and D. Beysens, J. Chem. Phys. **100**, 604 (1994).
[51] G. Zalczer, A. Bourgou, and D. Beysens, Phys. Rev A **28**, 440 (1983).
[52] *CRC Handbook of Chemistry and Physics*, 63rd ed., edited by Robert C. Weast (Chemical Rubber Company, Boca Raton, FL, 1982).
[53] D. Beysens, A. Bourgou, and P. Calmettes, Phys. Rev. A **26**, 3589 (1982).
[54] D. Atack and O. K. Rice, Discuss. Faraday Soc. **15**, 210 (1953).
[55] D. Beysens and D. Esteve, Phys. Rev. Lett. **54**, 2124 (1985).
[56] M. A. Handschy, R. C. Mockler, and W. J. O'Sullivan, Chem. Phys. Lett. **76**, 172 (1980). The first 15 data points were refitted with $\beta = 0.325$ to give $\Delta n = 0.288 t^{\beta}$.
[57] E. Gulari, A. F. Collings, R. L. Schmidt, and C. J. Pings, J. Chem. Phys. **56**, 6169 (1972). Gulari *et al.* measured 2.0 ± 0.2 and 2.92 ± 0.19 Å for the correlation length amplitude in the one-phase region. In Ref. [5] we find that 2.5 Å works well.
[58] J. Rouch, P. Tartaglia, and S. H. Chen, Phys. Rev. A **37**, 3046 (1988). In this reference, $\xi_{0+} = 3.54$ Å was measured for NH. In Ref. [51] $\xi_{0+} = 2.65$ Å was measured. In Ref. [5] we found that $\xi_{0+} = 3.1$ Å worked well.
[59] J. J. Jasper, J. Phys. Chem. Ref. Data **1**, 841 (1972).